

Excited-State Switching between Ligand-Centered and Charge Transfer Modulated by Metal–Carbon Bonds in Cyclopentadienyl Iridium Complexes

Joseph C. Deaton,^{*,†} Chelsea M. Taliaferro,[†] Catherine L. Pitman,^{‡,||} Rafał Czerwieńiec,[§] Elena Jakubikova,[†] Alexander J. M. Miller,^{*,‡,||} and Felix N. Castellano^{*,†,||}

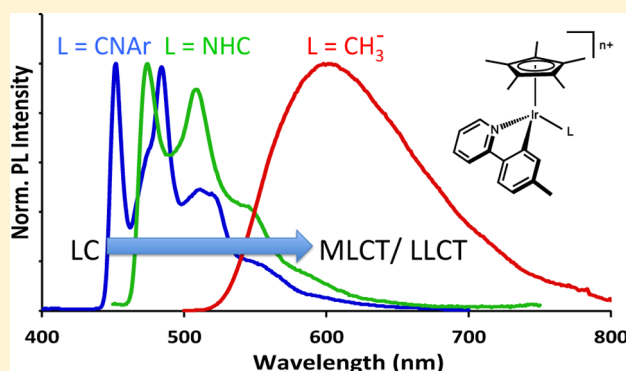
[†]Department of Chemistry, North Carolina State University, Raleigh, North Carolina 27695-8204, United States

[‡]Department of Chemistry, University of North Carolina at Chapel Hill, Chapel Hill, North Carolina 27599-3290, United States

[§]Institut für Physikalische und Theoretische Chemie, Universität Regensburg, Universitätstrasse 31, D-93040 Regensburg, Germany

Supporting Information

ABSTRACT: Three series of pentamethylcyclopentadienyl (Cp^{*}) Ir(III) complexes with different bidentate ligands were synthesized and structurally characterized, [Cp^{*}Ir(tpy)L]ⁿ⁺ (tpy = 2-tolylpyridinato; n = 0 or 1), [Cp^{*}Ir(piq)L]ⁿ⁺ (piq = 1-phenylisoquinolinato; n = 0 or 1), and [Cp^{*}Ir(bpy)L]^{m+} (bpy = 2,2'-bipyridine; m = 1 or 2), featuring a range of monodentate carbon-donor ligands within each series [L = 2,6-dimethylphenylisocyanide; 3,5-dimethylimidazol-2-ylidene (NHC); methyl]. The spectroscopic and photophysical properties of these molecules and those of the photocatalyst [Cp^{*}Ir(bpy)H]⁺ were examined to establish electronic structure–photophysical property relationships that engender productive photochemical reactivity of this hydride and its methyl analogue. The Ir(III) chromophores containing ancillary CNAr ligands exhibited features anticipated for predominantly ligand-centered (LC) excited states, and analogues bearing the NHC ancillary exhibited properties consistent with LC excited states containing a small admixture of metal-to-ligand charge-transfer (MLCT) character. However, the molecules featuring anionic and strongly σ -donating methyl or hydride ligands exhibited photophysical properties consistent with a high degree of CT character. Density functional theory calculations suggest that the lowest energy triplet states in these complexes are composed of a mixture of MLCT and ligand-to-ligand CT originating from both the Cp^{*} and methyl or hydride ancillary ligands. The high degree of CT character in the triplet excited states of methyliridium complexes bearing C[∧]N-cyclometalated ligands offer a striking contrast to the photophysical properties of pseudo-octahedral structures *fac*-Ir(C[∧]N)₃ or Ir(C[∧]N)₂(acac) that have lowest-energy triplet excited states characterized as primarily LC character with a more moderate MLCT admixture.



INTRODUCTION

The key to obtaining bright phosphorescence from iridium(III) complexes is the presence of Ir–C bonds that have strong σ -donor character in addition to a chromophoric ligand featuring low-lying π^* orbitals.^{1,2} The archetypal complex *fac*-Ir(ppy)₃ (ppy = 2-phenylpyridine) contains an Ir–C bond along each of the three principal axes of the molecule^{3,4} and exhibits an extraordinary quantum yield close to unity.^{5,6} The empty π^* orbitals are the Franck–Condon termination point for both metal-to-ligand charge transfer (MLCT) and ligand-centered (LC) π – π^* transitions. The strong σ -donor ligands induce a large ligand field splitting between the filled $d\pi$ orbitals and the empty $d\sigma^*$ orbitals in these d^6 chromophores so that the ³MLCT/LC states are the lowest energy excited states, rendering the higher lying ligand field excited states irrelevant. Stronger σ -donor ligands substantially increase electron density on the metal center, raising the energy of

the $d\pi$ orbitals so that the zero-order MLCT energy is decreased. As a consequence, additional MLCT character mixes through configuration interaction with the emissive ³LC excited state. The proportion of the MLCT composition with respect to LC character of the triplet excited state determines the characteristic photophysical properties, including excited-state energetics, photoluminescence emission bandshape, and radiative decay times.^{7–10}

Myriad classes of organometallic Ir(III) complexes featuring strong photoluminescence emission have recently been summarized.¹⁰ Beyond *fac*-Ir(C[∧]N)₃, the most common structural motifs are Ir(C[∧]N)₂(L[∧]X) and [Ir(C[∧]N)₂(N[∧]N)]⁺, where C[∧]N is a monoanionic bidentate ligand featuring a C-donor obtained from cyclometalation of a pyridine derivative

Received: September 26, 2018

(e.g., ppy), $L^{\wedge}X$ is a monoanionic bidentate ancillary ligand, and $N^{\wedge}N$ is a diimine ligand (e.g., bpy). In the $[\text{Ir}(\text{C}^{\wedge}\text{N})_2(\text{N}^{\wedge}\text{N})]^+$ class, the lowest energy π^* orbitals are usually found on the diimine fragment, rather than the $\text{C}^{\wedge}\text{N}$ chelate, and the nature of the emissive state is then best described as comprising ligand-to-ligand charge transfer (LLCT) as well as MLCT character because of ground-state d-orbital mixing with the $\text{C}^{\wedge}\text{N}$ -ligand π system.^{11–14} In the present paper, we use the general descriptor of charge transfer (CT) until a more specific characterization can be made later in the presentation. Analogous molecules where the $\text{C}^{\wedge}\text{N}$ -cyclometalating ligand is replaced by ligands such as $\text{C}^{\wedge}\text{C}$., where C: represents an N-heterocyclic carbene donor, comprise yet another important class of highly phosphorescent Ir(III) complexes.^{10,15,16}

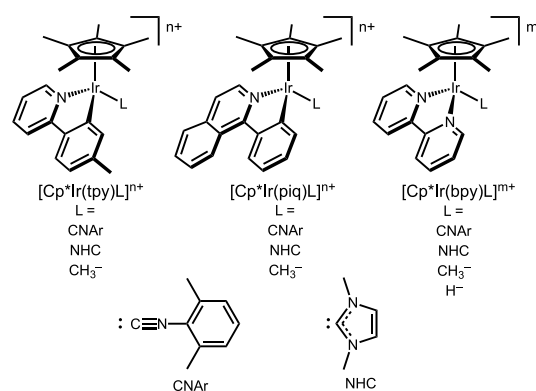
Vigorous investigation of Ir(III) phosphors has been driven largely by the commercialization of organic-light-emitting diodes (OLEDs) for displays and solid-state lighting wherein these molecules serve as emitters.^{17,18} With an impressive structural diversity and tunable photophysical and photochemical properties, these chromophores have been applied extensively in solar energy conversion schemes and as “photoredox” catalysts in organic synthesis,^{19–22} among many promising light-emission and photochemistry inspired applications.²³

Iridium(III) complexes containing a η^5 -cyclopentadienyl subunit have received comparatively little attention for their photophysical properties. There were early reports of weak photoluminescence with lifetimes near 80 ns for complexes of the type $[\text{Cp}^*\text{Ir}(\text{N}^{\wedge}\text{N})\text{H}]^+$, $\text{N}^{\wedge}\text{N}$ = bpy or phen.^{24,25} These hydrides exhibit striking photochemical reactivity, as first recognized in the context of a photochemical water–gas shift reaction.^{26–28} Recently, there has been renewed interest in these hydrido complexes for their photocatalytic properties,²⁹ including hydrogen generation from water^{30,31} or formate,³² and hydride transfer to 1-methylnicotinamide.³³ The methyl analogue, $[\text{Cp}^*\text{Ir}(\text{bpy})(\text{CH}_3)]^+$, has also been isolated recently and reported to generate ethane and other small hydrocarbons upon exposure to visible light.³⁴

Even the weak photoluminescence emission and short luminescence lifetimes of the hydride and methyl complexes were intriguing, given that their structure differs from leading Ir(III) phosphors. It immediately became evident that additional structurally related molecules would need to be identified and investigated to establish systematic structure–photophysical property trends to glean insight into why these molecules show photoluminescence at room temperature in the first place.

To this end, we set out to synthesize a range of newly conceived $\text{Cp}^*\text{Ir}(\text{III})$ complexes with varying bidentate and monodentate ligands to carry out a detailed photophysical study and make comparisons to the known complexes $[\text{Cp}^*\text{Ir}(\text{bpy})(\text{CH}_3)]^+$ and $[\text{Cp}^*\text{Ir}(\text{bpy})\text{H}]^+$. We have prepared three distinct series of Ir(III) complexes based on the identity of the bidentate chromophoric ligand (Scheme 1): $[\text{Cp}^*\text{Ir}(\text{tpy})\text{L}]^{n+}$ (tpy = 2-tolylpyridinato; $n = 0, 1$), $[\text{Cp}^*\text{Ir}(\text{piq})\text{L}]^{n+}$ (piq = 1-phenylisoquinolinato; $n = 0, 1$), and $[\text{Cp}^*\text{Ir}(\text{bpy})\text{L}]^{m+}$ (bpy = 2,2'-bipyridine; $m = 1, 2$), with each series featuring a range of monodentate carbon-donor ligands within each series [$L = 2,6$ -dimethylphenylisocyanide (CNAr); 3,5-dimethylimidazol-2-ylidene (NHC); methyl]. Absorption and photoluminescence spectra, including temperature-dependent photoluminescence intensity decay time constants, have been

Scheme 1. Chemical Structure Diagrams of the Three Series of Ir(III) Molecules Investigated and of the Monodentate Ancillary Ligands, L



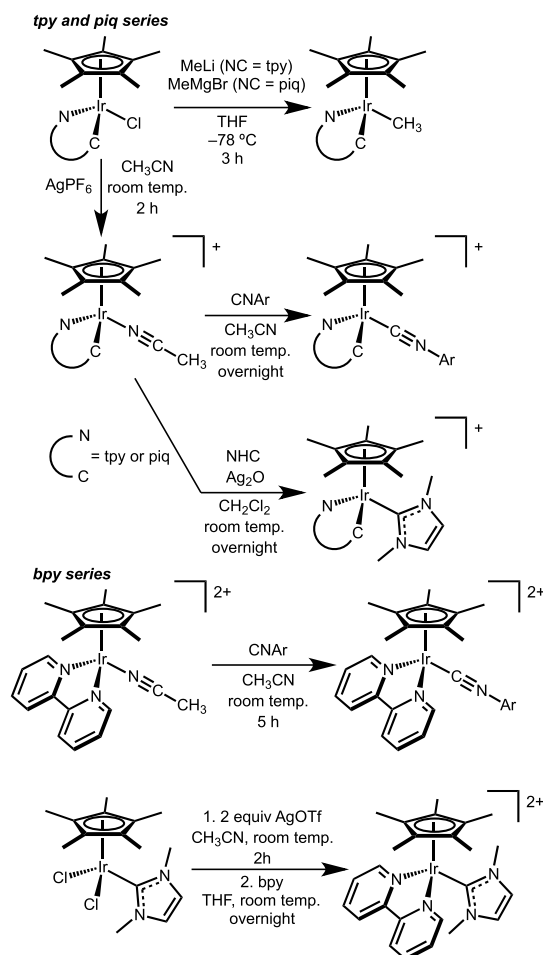
obtained for samples of each complex in Scheme 1 dilutely doped into polymethylmethacrylate (PMMA), a polymer host that has often been used to avoid the phase transitions of solvents in variable temperature studies.

We hypothesized that replacing the $\text{N}^{\wedge}\text{N}$ chelating bpy ligand with $\text{C}^{\wedge}\text{N}$ -cyclometalating ligands would boost emission quantum yield by introducing a chromophoric ligand that also contributes an Ir–C bond. Tpy was selected to facilitate comparisons to the landmark study⁷ by Thompson and co-workers on the emission-shifting properties of the $L^{\wedge}X$ ancillary ligands measured for a large series $\text{Ir}(\text{tpy})_2(L^{\wedge}X)$. 1-Phenylisoquinoline was selected as a $\text{C}^{\wedge}\text{N}$ ligand to provide a chromophore with lower triplet energy. The well-known red emitters^{35,36} *fac*- $\text{Ir}(\text{piq})_3$ and $\text{Ir}(\text{piq})_2(\text{acac})$ offer points of comparison for the results generated here. Monodentate ancillary ligands, L, were chosen to cover a wide range of bonding properties while maintaining a carbon donor. The strong π -backbonding neutral ligand CNAr and the strong σ -donating neutral ligand NHC were compared with the strongly σ -donating anionic methyl ligand to investigate how the extent of CT versus LC character can be affected from this single coordination site. Finally, the series $[\text{Cp}^*\text{Ir}(\text{bpy})\text{L}]^{m+}$ ($m = 1$ and 2) was compared with $[\text{Cp}^*\text{Ir}(\text{bpy})\text{H}]^+$ to enable a qualitative ranking of the donor strength of the hydride ligand in this molecular framework.

RESULTS AND DISCUSSION

Synthesis. The chloro complexes $\text{Cp}^*\text{Ir}(\text{C}^{\wedge}\text{N})\text{Cl}$ ($\text{C}^{\wedge}\text{N}$ = tpy or piq), prepared according to the method developed by Li et al.³⁷ for the analogue $\text{Cp}^*\text{Ir}(\text{ppy})\text{Cl}$, proved to be versatile starting materials for the synthesis of both the tpy and piq series of complexes (Scheme 2). The methyl complexes $\text{Cp}^*\text{Ir}(\text{C}^{\wedge}\text{N})(\text{CH}_3)$ ($\text{C}^{\wedge}\text{N}$ = tpy or piq) were obtained by reaction of the chloro complexes with methyl lithium ($\text{C}^{\wedge}\text{N}$ = tpy) or CH_3MgBr ($\text{C}^{\wedge}\text{N}$ = piq).³⁸ The acetonitrile complexes $[\text{Cp}^*\text{Ir}(\text{C}^{\wedge}\text{N})(\text{NCCH}_3)][\text{PF}_6]$ were obtained by chloride abstraction with AgPF_6 in acetonitrile, and the isocyanide complexes $[\text{Cp}^*\text{Ir}(\text{C}^{\wedge}\text{N})(\text{CNAr})][\text{PF}_6]$ were subsequently obtained by ligand substitution of acetonitrile with 2,6-dimethylphenylisocyanide. The N-heterocyclic carbene complexes $[\text{Cp}^*\text{Ir}(\text{C}^{\wedge}\text{N})(\text{NHC})][\text{PF}_6]$ were prepared by allowing the acetonitrile complexes to react with 3,5-dimethylimidazolium iodide and Ag_2O in dichloromethane solutions protected from light.

Scheme 2. Synthesis of the New Ir(III) Chromophores



The bipyridine complexes $[\text{Cp}^*\text{Ir}(\text{bpy})(\text{CH}_3)][\text{PF}_6]$ ³⁴ and $[\text{Cp}^*\text{Ir}(\text{bpy})\text{H}][\text{PF}_6]$ ³⁵ were synthesized as previously reported. The isocyanide complex $[\text{Cp}^*\text{Ir}(\text{bpy})(\text{CNAr})][\text{PF}_6]_2$ was obtained by addition of 2,6-dimethylphenylisocyanide to the known acetonitrile complex $[\text{Cp}^*\text{Ir}(\text{bpy})(\text{NCCH}_3)]_2[\text{PF}_6]_2$.³⁹ A different synthetic route was taken to prepare the N-heterocyclic carbene complex. The starting material $\text{Cp}^*\text{Ir}(\text{NHC})\text{Cl}_2$, prepared by a modified literature method,⁴⁰ was converted to the bis acetonitrile complex $[\text{Cp}^*\text{Ir}(\text{NHC})(\text{NCCH}_3)_2][\text{CF}_3\text{SO}_3]_2$ via halide abstraction using AgCF_3SO_3 , followed by stirring with bpy at room temperature to produce $[\text{Cp}^*\text{Ir}(\text{bpy})(\text{NHC})][\text{CF}_3\text{SO}_3]_2$. The triflate counter ion was employed in this case to improve solubility. NMR characterization of all compounds is seen in Figures S1–21.

Absorption and Photoluminescence Emission Spectra. Overview. Key spectral features of the three series of complexes are collected in Table 1 and discussed in detail in the following paragraphs. In summary, across each series of complexes identified by a different bidentate chromophoric ligand, the spectral features and nature of the excited state shifted markedly as a function of the monodentate ligand. The features of each CNAr complex were characteristic of a highly LC lowest excited state, those of each NHC complex were characteristic of a still predominantly LC excited state but with an increased MLCT admixture, while the methyl complexes exhibited drastically different spectral features indicative of a very high CT character. The spectral features of the photocatalyst $[\text{Cp}^*\text{Ir}(\text{bpy})\text{H}]^+$ were very similar to those of

Table 1. Spectroscopic Features of the Ir(III) molecules in This Study

complex	ϵ , $S_0 \rightarrow T_1$ ($\text{M}^{-1} \text{cm}^{-1}$) ^a	$E_{(0-0)}$, $S_0 \rightarrow T_1$ (cm^{-1}) ^a	λ_{max} Em. 77 K (nm) ^e	$I_{(0-1)}/I_{(0-0)}$ ^{e,j} 77 K
$[\text{Cp}^*\text{Ir}(\text{tpy})(\text{CNAr})]^+$	10	22 173 ^c	454 ^f	0.99
$[\text{Cp}^*\text{Ir}(\text{tpy})(\text{NHC})]^+$	57	21 552 ^c	474 ^f	0.89
$\text{Cp}^*\text{Ir}(\text{tpy})(\text{CH}_3)$	NR ^b	18 975 ^d	603 ^g	NA ^g
$[\text{Cp}^*\text{Ir}(\text{piq})(\text{CNAr})]^+$	4	18 622 ^c	601 ^h	1.20
$[\text{Cp}^*\text{Ir}(\text{piq})(\text{NHC})]^+$	45	17 544 ^c	591 ^f	0.71
$\text{Cp}^*\text{Ir}(\text{piq})(\text{CH}_3)$	NR ^b	16 207 ^d	687 ^g	NA ^g
$[\text{Cp}^*\text{Ir}(\text{bpy})(\text{CNAr})]^{2+}$	10	22 676 ^c	471 ^h	1.27
$[\text{Cp}^*\text{Ir}(\text{bpy})(\text{NHC})]^{2+}$	88	22 222 ^c	NA ⁱ	NA ⁱ
$[\text{Cp}^*\text{Ir}(\text{bpy})(\text{CH}_3)]^+$	NR ^b	18 282 ^d	609 ^g	NA ^g
$[\text{Cp}^*\text{Ir}(\text{bpy})(\text{H})]^+$	NR ^b	18 315 ^d	622 ^g	NA ^g

^aIn methylene chloride solution at 295 K except for $[\text{Cp}^*\text{Ir}(\text{bpy})\text{H}]^+$ was in acetonitrile. ^b $S_0 \rightarrow T_1$ absorption was not resolved. ^cEnergy for the peak maximum of $S_0 \rightarrow T_1$ origin band. ^d $E_{0,0}$ estimated from the crossing point on the wavelength axis of the tangent to leading edge of broad emission band. ^e0.5 wt % in PMMA host except for $[\text{Cp}^*\text{Ir}(\text{tpy})(\text{NHC})]^+$ and $[\text{Cp}^*\text{Ir}(\text{piq})(\text{NHC})]^+$ were $\sim 5 \times 10^{-5}$ M in frozen $\text{CH}_2\text{Cl}_2/2\text{MeTHF}$ glass (1:20 or 1:10, respectively). ^f λ_{max} occurred on the origin band of vibrationally structured emission. ^gBroad, unstructured emission. ^h λ_{max} occurred on the first vibrational sideband of structured emission. ⁱNonemissive. ^jRatio of steady-state emission intensity of the first vibrational sideband to that of the origin band.

the methyl analogue, as noted in a preliminary study of the methyl complex.³⁴ Emission-shifting by tuning electron-withdrawing/-donating capacity of ancillary ligands is well-established,^{7,41–44} but the present set of materials demonstrates tuning over an extreme range, and with just one monodentate ancillary ligand. Perhaps most intriguing, the C^*N -cyclometallates in combination with the methyl ancillary ligand exhibit characteristics of a very highly CT emissive state, whereas typical cyclometallates with the same chromophoric ligands, that is, $\text{fac-Ir}(\text{C}^*\text{N})_3$ or $\text{Ir}(\text{C}^*\text{N})_2(\text{acac})$, exhibit characteristics that are largely LC with moderate MLCT admixture.

$[\text{Cp}^*\text{Ir}(\text{tpy})\text{L}]^{n+}$ Series. The tpy series will be considered in detail first. The absorption spectrum of $[\text{Cp}^*\text{Ir}(\text{tpy})(\text{CNAr})][\text{PF}_6]$ in CH_2Cl_2 is included in Figure 1a along with the emission spectrum and the excitation spectrum in the origin region in PMMA host at 77 K. The absorption bands having higher extinction coefficients typical for singlet excited states were not more specifically assigned because there are three different organic ligands. The lowest energy of these bands ($S_0 \rightarrow S_1$) occurs at $\lambda_{\text{max}} = 336 \text{ nm}$ ($9300 \text{ M}^{-1} \text{cm}^{-1}$). A very weak shoulder feature in the absorption spectrum at 420 nm and a lowest energy band at 451 nm were apparent in a more concentrated solution. The 77 K excitation spectrum confirmed that the two weak absorption bands belong to the emissive complex. The extremely low extinction coefficient ($10 \text{ M}^{-1} \text{cm}^{-1}$) of the origin band ($S_0 \rightarrow T_1$) indicates that the lowest energy excited state is a triplet that is highly LC. This is

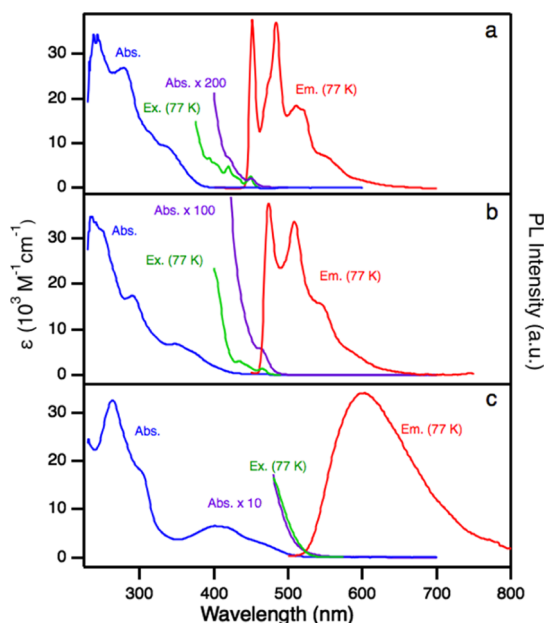


Figure 1. (a) Absorption (295 K, CH_2Cl_2), excitation (77 K, $\lambda_{\text{det}} = 485$ nm), and emission (77 K, $\lambda_{\text{ex}} = 380$ nm) spectra of $[\text{Cp}^*\text{Ir}(\text{tpy})(\text{CNAr})][\text{PF}_6]$ in PMMA. (b) Absorption (295 K, CH_2Cl_2), excitation (77 K, $\lambda_{\text{det}} = 510$ nm) and emission (77 K, 1:20 CH_2Cl_2 : 2-methyl-tetrahydrofuran (THF) glass, $\lambda_{\text{ex}} = 372$ nm) spectra of $[\text{Cp}^*\text{Ir}(\text{tpy})(\text{NHC})][\text{PF}_6]$. (c) Absorption (295 K, CH_2Cl_2), excitation ($\lambda_{\text{det}} = 615$ nm), and emission (77 K, PMMA, $\lambda_{\text{ex}} = 470$ nm) spectra of $\text{Cp}^*\text{Ir}(\text{tpy})(\text{CH}_3)$.

because the oscillator strength of the formally spin-forbidden transition depends upon the strength of the spin–orbit coupling (SOC) interaction and is much stronger when MLCT states are involved because of the large SOC constant for heavy atoms.^{7,45} The weak bands above the origin in energy likely comprise a vibrational progression in that excited state. The origin band of the emission spectrum overlaps with the origin band of the absorption spectrum, giving good evidence that emission is occurring from the same excited state associated with absorption. In qualitative terms, the large window evident in Figure 1 between the $S_0 \rightarrow S_1$ absorption region and the $S_0 \rightarrow T_1$ origin band is another sign of a LC lowest excited state because a large S_1 – T_1 splitting arises from a large electron exchange interaction when the starting and arriving orbitals are spatially close, as compared to MLCT states for which there is a large translation of the excited electron.⁴⁶ The highly structured emission is the most readily recognizable hallmark of an LC emissive state. In particular, a larger ratio of the first vibronic emission sideband intensity to the origin band intensity ($I_{(0-1)}/I_{(0-0)}$) indicates a higher degree of LC character of the emissive state because the ligand vibrations are more strongly coupled to the electronic transition when it is predominantly localized on the ligand and because the LC transition (π – π^*) involves promotion of an electron from a bonding to antibonding orbital, resulting in a large displacement of the excited-state potential energy well along the normal coordinate.

In a landmark study⁷ on a large series of complexes $\text{Ir}(\text{tpy})_2(\text{L}^\wedge\text{X})$, Thompson and co-workers found that introducing electron-withdrawing groups into the ancillary ligand L^\wedgeX led to progressive blue shifts in the emission, decreased the extinction coefficient of the absorption origin band, and increased the $I_{(0-1)}/I_{(0-0)}$ ratio. The interpretation

given for these trends was that the decreasing electron density on the metal lowers the energy of the starting d-orbital for the lowest MLCT transition, which increases the energy for the MLCT transition and results in less MLCT admixture into the LC excited state. The spectroscopic properties of $[\text{Cp}^*\text{Ir}(\text{tpy})(\text{CNAr})]^+$ and the $\text{Ir}(\text{tpy})_2(\text{L}^\wedge\text{X})$ series may be compared because they share in common the same chromophoric tpy ligand. On the basis of the low extinction of the origin band of $[\text{Cp}^*\text{Ir}(\text{tpy})(\text{CNAr})]^+$ and high $I_{(0-1)}/I_{(0-0)}$ (0.99), the emission of this complex may be ranked as more highly LC than any of those in the report on the $\text{Ir}(\text{tpy})_2(\text{L}^\wedge\text{X})$ series.⁷ In particular, the origin band of $[\text{Ir}(\text{tpy})_2(\text{CN}-t\text{-Bu})][\text{CF}_3\text{SO}_3]$ at 452 nm was reported to have a higher extinction ($30 \text{ M}^{-1} \text{ cm}^{-1}$) and lower $I_{(0-1)}/I_{(0-0)}$ (0.64). (In a closely related comparison, $I_{(0-1)}/I_{(0-0)}$ of about 1.06 may be seen in the published⁴⁷ solution spectrum of $[\text{Ir}(\text{ppy})_2(\text{CNAr})_2]^+$ which contains the same aryl isocyanide as in the present study but a slightly different chromophoric C^N-ligand.) Strong π -back-bonding with the CNAr ligand is undoubtedly responsible for the high LC character observed in the present case.

When the CNAr ligand was replaced by an N-heterocyclic carbene in $[\text{Cp}^*\text{Ir}(\text{tpy})(\text{NHC})][\text{PF}_6]$, the origin bands of absorption (464 nm) and emission (474 nm) were red-shifted and the $\epsilon(S_0 \rightarrow T_1)$ increased to $57 \text{ M}^{-1} \text{ cm}^{-1}$, whereas $I_{(0-1)}/I_{(0-0)}$ (0.89) decreased but was still quite high (Figure 1b, Table 1). The red shift, higher $\epsilon(S_0 \rightarrow T_1)$, and lower $I_{(0-1)}/I_{(0-0)}$ all indicate modestly higher CT character in the emissive state of the NHC complex than in the CNAr analogue. Higher $\epsilon(S_0 \rightarrow T_1)$ indicates that specifically there is more MLCT character in the lowest energy excited state in this complex than in the preceding one containing the CNAr ancillary ligand. The increased CT character is mainly due to reduction of the π -backbonding capacity of the ancillary NHC ligand compared with that of the CNAr ligand. It may be concluded that the lowest excited state in $[\text{Cp}^*\text{Ir}(\text{tpy})(\text{NHC})]^+$ does not possess as much CT character as that of $\text{Ir}(\text{tpy})_2(\text{acac})$ because of large differences relative to reported emission energy, $\epsilon(S_0 \rightarrow T_1)$, and $I_{(0-1)}/I_{(0-0)}$ for the latter complex.⁷ A direct spectrochemical assessment of the relative electron donating ability of the Cp^* moiety is difficult because its coordination mode substantially differs from that of C^N ligands. However, a cationic complex, $[\text{Ir}(\text{tpy})_2(\text{pyrazole})_2]^+$, exhibited higher $\epsilon(S_0 \rightarrow T_1)$ ($170 \text{ M}^{-1} \text{ cm}^{-1}$), lower $E_{(0-0)}$ ($21\,186 \text{ cm}^{-1}$, or 472 nm), and smaller $I_{(0-1)}/I_{(0-0)}$ (0.33).⁷ Thus, in spite of having two weak donor monodentate ligands, its excited state contains more MLCT character at the expense of LC character than the one in $[\text{Cp}^*\text{Ir}(\text{tpy})(\text{NHC})]^+$. This comparison qualitatively suggests that the electron donating ability of Cp^* π system should be considered less than that of a (second) C^N ligand.

Employing the anionic methyl ligand as the monodentate ancillary in $\text{Cp}^*\text{Ir}(\text{tpy})(\text{CH}_3)$ results in dramatic changes in spectroscopic features relative to those of the previous two complexes. Most striking, the emission is greatly red-shifted ($\lambda_{\text{max}} = 603$ nm) and broadened; no vibronic features, not even shoulders, are apparent (Figure 1c). The absorption is also strongly red-shifted, and there is a distinct set of overlapping bands from 350 to 500 nm (ϵ at 402 nm = $6550 \text{ M}^{-1} \text{ cm}^{-1}$) which may be assigned as the ¹MLCT region. The energy gap between the ¹MLCT absorption and the emission origin was reduced. The $S_0 \rightarrow T_1$ absorption was not resolved, hindering accurate estimation of the energy of the origin band and precluding estimation of the extinction coefficient of the origin

absorption. A crude estimate of the $S_0 \rightarrow T_1$ origin was taken from the crossing point of the tangent to the emission band and the wavelength axis (Table 1). The red shift of the origin relative to that of $[\text{Cp}^*\text{Ir}(\text{tpy})(\text{NHC})]^+$ is thus estimated to be about 2580 cm^{-1} . The very broad bandshape of the emission is evidence of a dominantly CT transition because now the electronic transition is additionally coupled to metal–ligand vibrations that are low in energy ($<600 \text{ cm}^{-1}$).^{9,46,48} The very high CT character of the lowest excited state in $\text{Cp}^*\text{Ir}(\text{tpy})(\text{CH}_3)$ relative to that in $[\text{Cp}^*\text{Ir}(\text{tpy})(\text{NHC})]^+$ may be explained by the reduction in charge of the complex and very strong donor property of the methyl ligand. It may also be concluded that the emission from $\text{Cp}^*\text{Ir}(\text{tpy})(\text{CH}_3)$ has much higher CT character than that of *fac*- $\text{Ir}(\text{tpy})_3$ and $\text{Ir}(\text{tpy})_2(\text{acac})$ because the latter two emit at higher energy in the green spectral region and exhibit a vibrational shoulder or sideband. It should not be assumed, however, that this increased CT character is entirely the MLCT character but may comprise a substantial amount of LLCT character as well. The inability to resolve the $S_0 \rightarrow T_1$ transition and measure its extinction coefficient precludes making a relative assessment of the degree of MLCT character at this point.

The complexes with the neutral donor ligands, $[\text{Cp}^*\text{Ir}(\text{tpy})\text{L}]^+$ (L = CNAr and NHC), were nonemissive above about 120 K. Even $\text{Cp}^*\text{Ir}(\text{tpy})(\text{CH}_3)$, which features an additional strong σ -donating methyl ligand, was essentially nonemissive above 200 K. The lack of emission is in striking contrast to that of the $\text{Ir}(\text{tpy})_2(\text{L}^{\wedge}\text{X})$ complexes, which generally exhibit strong emission at room temperature. One explanation for the different temperature dependence is that the $[\text{Cp}^*\text{Ir}(\text{tpy})\text{L}]^{n+}$ complexes possess a relatively weak, low-symmetry ligand field that places a nonradiative d–d state not far in energy above that of the emissive state, even in the case of the methyl complex. This weaker ligand field could stem from the electron donation by the ligands not being directly aligned along three mutually orthogonal axes of the complexes. Alternatively, the weak field may result from less electron-donating ability of the Cp^* moiety or a combination of these two factors. To probe this conclusion further, the cyclometalating ligand 1-phenylisoquinoline (piq) was employed to produce a series of three complexes analogous to the tpy series, but with a lower energy triplet emitting state that would be further separated from any low-lying d–d states.

$[\text{Cp}^*\text{Ir}(\text{piq})\text{L}]^{n+}$ Series. Initial examinations of the series of piq complexes reveal weak emission in solution at room temperature and fairly bright emission when restrained in a PMMA host matrix, in accord with better separation of emissive states and d–d states. The trends in spectral features as a function of monodentate ancillary ligand for the piq series (Figure 2a–c and Table 1) were similar to those observed of the tpy series. The values of $\epsilon(S_0 \rightarrow T_1)$, $E_{(0-0)}$ ($S_0 \rightarrow T_1$), and $I_{(0-1)}/I_{(0-0)}$ lead to the conclusion that the emissive state for the CNAr complex is highly LC and that for NHC complex has more CT character, but is still strongly LC. The broad, featureless, and deeply red-shifted emission for the methyl complex is indicative of an emissive state that is highly CT in nature. Comparison to the energy of the emission origin and relative intensity of vibronic shoulder or sideband seen in the published^{35,36} spectra for *fac*- $\text{Ir}(\text{piq})_3$ and $\text{Ir}(\text{piq})_2(\text{acac})$ leads to a rank order that these comparatives have more CT character in their lowest excited state than $[\text{Cp}^*\text{Ir}(\text{piq})(\text{NHC})]^+$ but much less than that for $\text{Cp}^*\text{Ir}(\text{piq})(\text{CH}_3)$.

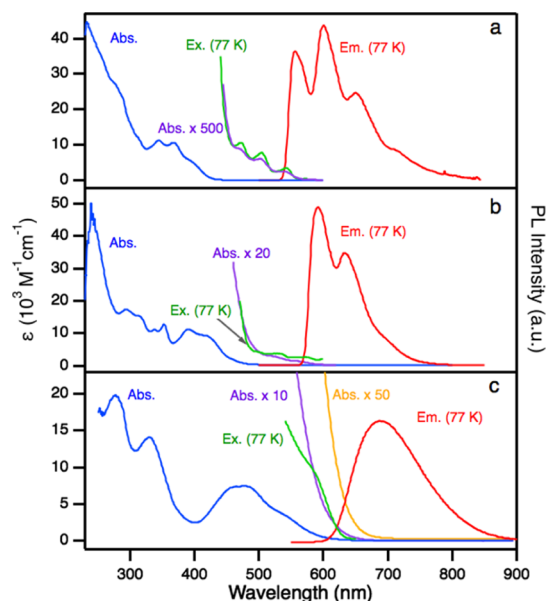


Figure 2. (a) Absorption (295 K, CH_2Cl_2), excitation (77 K, $\lambda_{\text{det}} = 600 \text{ nm}$), and emission (77 K, PMMA, $\lambda_{\text{ex}} = 425 \text{ nm}$) spectra of $[\text{Cp}^*\text{Ir}(\text{piq})(\text{CNAr})][\text{PF}_6]$. (b) Absorption (295 K, CH_2Cl_2), excitation (77 K $\lambda_{\text{det}} = 625 \text{ nm}$), and emission (77 K, 1:10 CH_2Cl_2 : 2-methyl-THF glass, $\lambda_{\text{ex}} = 475 \text{ nm}$) spectra of $[\text{Cp}^*\text{Ir}(\text{piq})(\text{NHC})][\text{PF}_6]$. (c) Absorption (295 K, CH_2Cl_2), excitation (77 K, $\lambda_{\text{det}} = 670 \text{ nm}$), and emission (77 K, PMMA, $\lambda_{\text{ex}} = 520 \text{ nm}$) spectra of $\text{Cp}^*\text{Ir}(\text{piq})(\text{CH}_3)$.

$[\text{Cp}^*\text{Ir}(\text{bpy})\text{L}]^{m+}$ Series. Proceeding to the bpy series, the net charge of the complexes increases by 1 because the cyclometalating ligand has been replaced with the neutral diimine. $[\text{Cp}^*\text{Ir}(\text{bpy})(\text{CNAr})][\text{PF}_6]_2$ was only weakly emissive once below 100 K. The absorption and 77 K emission spectra of $[\text{Cp}^*\text{Ir}(\text{bpy})(\text{CNAr})][\text{PF}_6]_2$ are shown in Figure 3a.

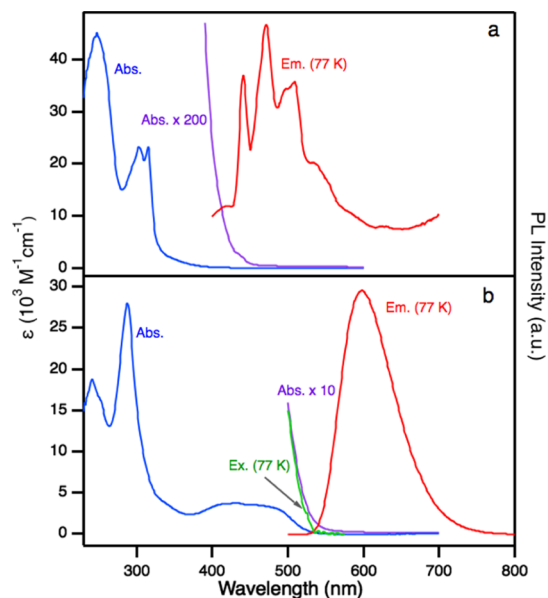


Figure 3. (a) Absorption (295 K, CH_2Cl_2) and emission (77 K, PMMA, $\lambda_{\text{ex}} = 350 \text{ nm}$) spectra of $[\text{Cp}^*\text{Ir}(\text{bpy})(\text{CNAr})][\text{PF}_6]_2$. (b) Absorption (295 K, CH_2Cl_2), excitation (77 K, $\lambda_{\text{det}} = 625 \text{ nm}$), and emission (77 K, PMMA, $\lambda_{\text{ex}} = 470 \text{ nm}$) spectra of $[\text{Cp}^*\text{Ir}(\text{bpy})(\text{CH}_3)][\text{PF}_6]$.

Because the emission was weak relative to scattered light with the low temperature apparatus, we were unable to obtain a satisfactory excitation spectrum baseline at 77 K and therefore do not include it in Figure 3. However, the weak shoulder at 436 nm in absorption is reasonably assigned as the $S_0 \rightarrow T_1$ absorption of the complex because it occurs at the origin of the absorption and because it overlaps with the origin of the emission spectrum. Its small extinction ($10 \text{ M}^{-1} \text{ cm}^{-1}$) indicates a highly LC excited state. The highly structured emission spectrum wherein the vibrational sideband is even more intense than the origin band ($I_{(0-1)}/I_{(0-0)} = 1.3$) most clearly confirms the assignment of this state as highly LC. In fact, the emission spectrum closely matches in energy and bandshape of the published spectrum of $[\text{Ir}(\text{bpy})_3]^{3+}$ at 77 K in methanol–ethanol glass ($I_{(0-1)}/I_{(0-0)} \approx 1.36$).⁴⁹ (The free bpy ligand phosphorescence differs because many rotamers exist for the free ligand whereas in complexes the ligand is held planar.⁴⁹)

The NHC complex $[\text{Cp}^*\text{Ir}(\text{bpy})(\text{NHC})][\text{CF}_3\text{SO}_3]_2$ was nonemissive even at 77 K. Thus, only the absorption spectrum appears in Figure S22. The shoulder feature at the origin of the absorption (450 nm) likely arises from the $S_0 \rightarrow T_1$ transition because such an origin band was observed in all the other complexes having dominantly LC lowest excited states. The higher extinction of this feature ($88 \text{ M}^{-1} \text{ cm}^{-1}$) together with the small red shift (714 cm^{-1}) compared with that of $[\text{Cp}^*\text{Ir}(\text{bpy})(\text{CNAr})][\text{PF}_6]_2$ indicates that the lowest excited state in this complex is still highly LC in character, but not to the degree that it is in $[\text{Cp}^*\text{Ir}(\text{bpy})(\text{CNAr})][\text{PF}_6]_2$. The reason why the complex is nonemissive is not readily explained, but only a subtle factor would be enough to account for it being nonemissive relative to the $[\text{Cp}^*\text{Ir}(\text{bpy})(\text{CNAr})][\text{PF}_6]_2$ being barely emissive.

In remarkable contrast to the bpy complexes with the CNAr and NHC ligands, $[\text{Cp}^*\text{Ir}(\text{bpy})(\text{CH}_3)][\text{PF}_6]$ was emissive all the way up to room temperature, albeit weakly. Its absorption and 77 K excitation and emission spectra are shown in Figure 3b. The spectral features were drastically red-shifted in comparison to those of $[\text{Cp}^*\text{Ir}(\text{bpy})(\text{CNAr})][\text{PF}_6]_2$ and $[\text{Cp}^*\text{Ir}(\text{bpy})(\text{NHC})][\text{CF}_3\text{SO}_3]_2$ (Table 1). The broad, lowest energy absorption band with maximum extinction of $3690 \text{ M}^{-1} \text{ cm}^{-1}$ at 432 nm may be assigned as ${}^1\text{CT}$. No features that could be assigned to the $S_0 \rightarrow T_1$ transition could be resolved in the absorption spectrum. The emission spectrum was broad and featureless with no vibronic shoulder evident. The emission spectrum may be compared with that of $[\text{Ir}(\text{ppy})_2(\text{bpy})]^+$ wherein the bpy is the chromophoric ligand in CH_2Cl_2 solution at room temperature (as an aside, note that the rigidochromic effect in *crystalline* host shifts the bpy MLCT to higher energy, resulting in the LC ppy triplet becoming the emissive state).⁵⁰ This comparative complex exhibited a broad emission with $\lambda_{\text{max}} = 585 \text{ nm}$ in CH_2Cl_2 solution at room temperature, but when the complex was doped into PMMA host, the broad CT emission associated with the bpy ligand occurred at $\lambda_{\text{max}} = 532 \text{ nm}$.⁵⁰ Despite the presence of the two strong σ -donor cyclometalating ligands in the comparative complex, the excited state appears more highly CT in character for the present methyl complex because of its deeper red shift. The excited state in the comparative $[\text{Ir}(\text{ppy})_2(\text{bpy})]^+$ complex¹² and the $[\text{Cp}^*\text{Ir}(\text{bpy})(\text{CH}_3)]^+$ complex may have admixtures of MLCT and LLCT character (vide infra). As was the case with the $[\text{Cp}^*\text{Ir}(\text{C}^{\wedge}\text{N})(\text{CH}_3)]^+$ complexes, the inability to resolve the $S_0 \rightarrow T_1$ transition and measure its

extinction coefficient precludes making an experimental assessment of the relative MLCT character.

The absorption and 77 K excitation and emission spectra of $[\text{Cp}^*\text{Ir}(\text{bpy})\text{H}][\text{PF}_6]$ are shown in Figure S23 and are very similar to those observed for the methyl analogue (Figure 3b). The absorption band at 422 nm ($4010 \text{ M}^{-1} \text{ cm}^{-1}$) may be assigned as ${}^1\text{CT}$. The fact that the emission energies and bandshapes are so similar for the two compounds suggests that the excited states have a similar CT character and therefore that the methyl and hydride ligands are similarly strong σ -donors. The key point here is that each of these two ligands induce much higher CT character in the respective excited states than in those in other members of the bpy series or in comparative literature complexes as noted above. The same was true when the methyl ligand was used in combination with the cyclometalating ligands presented earlier relative to conventional Ir phosphors such as well-known OLED emitters.

Temperature Dependence of the Photophysical Properties. The complexes that displayed emission at room temperature were examined further through variable temperature studies. Emission spectra and decay times were obtained for the full series with piq as the chromophoric ligand, as well as $[\text{Cp}^*\text{Ir}(\text{bpy})(\text{CH}_3)][\text{PF}_6]$ and $[\text{Cp}^*\text{Ir}(\text{bpy})\text{H}][\text{PF}_6]$, from 77 to 300 K. A preliminary set of experiments from 1.7 to 100 K was also carried out for the latter two compounds. The quantum yields in PMMA host at 77 and 300 K for $\text{Cp}^*\text{Ir}(\text{piq})(\text{CH}_3)$, $[\text{Cp}^*\text{Ir}(\text{bpy})(\text{CH}_3)][\text{PF}_6]$, and $[\text{Cp}^*\text{Ir}(\text{bpy})\text{H}][\text{PF}_6]$ are listed in Table 2.

Table 2. Quantum Yields at 77 and 300 K for Selected Complexes at 0.5 wt % in PMMA

compound	77 K ^a	300 K ^b
$\text{Cp}^*\text{Ir}(\text{piq})(\text{CH}_3)$	$7 \pm 2 \times 10^{-2}$	$9 \pm 3 \times 10^{-3}$
$[\text{Cp}^*\text{Ir}(\text{bpy})(\text{CH}_3)][\text{PF}_6]$	$9 \pm 2 \times 10^{-2}$	$5 \pm 1 \times 10^{-4}$
$[\text{Cp}^*\text{Ir}(\text{bpy})\text{H}][\text{PF}_6]$	$3 \pm 2 \times 10^{-2}$	$3 \pm 2 \times 10^{-3}$

^aValues at 77 K measured with an absolute quantum yield instrument equipped with an integrating sphere. ^bValues at 300 K were estimated by scaling the 77 K values to the integrated emission intensity because the emission was below the error limits of the absolute quantum yield instrument.

In polymer hosts, spectral features are in general inhomogeneously broadened by local variations in the host–guest cage.^{46,51} Emission decays were correspondingly found to deviate from single exponential in polymer hosts and frozen solutions.^{52–54} Here, emission decays of the complexes in PMMA fit fairly close to single exponential decay at 77 K, but as the temperature was increased, the fits were no longer acceptable. Even fits to bi-exponential decays were not satisfactory at the higher temperatures. Therefore, the Kohlrausch function (eq 1), also known as the stretched exponential,^{55–59} was fit to the decays. In eq 1, the intensity is I and initial intensity is I_0 . The parameter τ is the decay time corresponding to the maximum amplitude within a distribution of decay times. Values of the parameter β less than 1 characterize the width of the distribution. When the parameter β is equal to 1, eq 1 reduces to the familiar single exponential decay. The average decay time is calculated from eq 2, for which the definition and values of the gamma function, $\Gamma(1/\tau)$, can be readily obtained.⁶⁰

$$I = I_0 \exp(-t/\tau)^\beta \quad (1)$$

$$\tau_{\text{ave}} = (\tau/\beta)\Gamma(1/\beta) \quad (2)$$

The average decay time, τ_{ave} , and the parameter β for $[\text{Cp}^*\text{Ir}(\text{piq})(\text{CNAr})][\text{PF}_6]$ are plotted versus temperature in Figure 4a. The decay time was fairly constant over the range

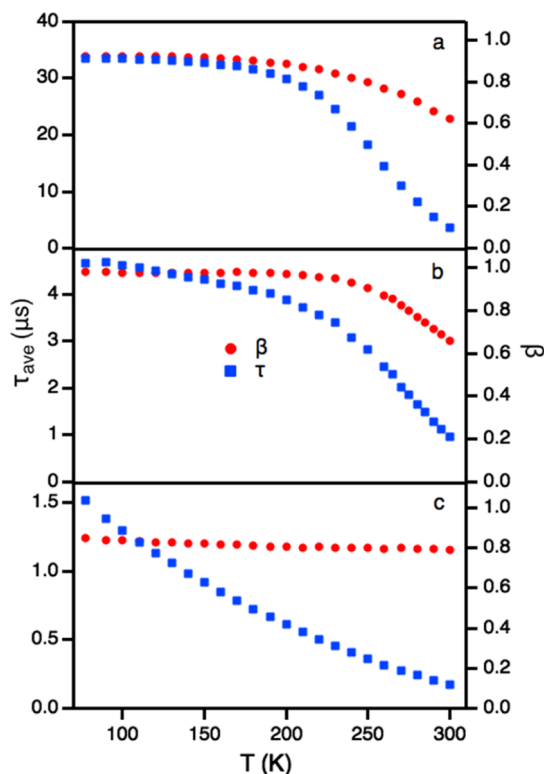


Figure 4. Temperature dependence of average emission decay time constants and the Kohlrausch parameter β for (a) $[\text{Cp}^*\text{Ir}(\text{piq})(\text{CNAr})][\text{PF}_6]$, (b) $[\text{Cp}^*\text{Ir}(\text{piq})(\text{NHC})][\text{PF}_6]$, and (c) $\text{Cp}^*\text{Ir}(\text{piq})(\text{CH}_3)$ measured in PMMA films.

77–150 K, and then begins a steep drop as temperature increased further. The parameter β tracked τ_{ave} , remaining fairly constant (0.91–0.93) from 77 to 150 K before falling steadily further below 1 as temperature increased. The β values that are close to 1 in the lower temperature regime indicate that the sample decay is close to single exponential, whereas β values further from 1 at higher temperatures indicate a widening distribution.

At thermal equilibrium and assuming only the triplet state is involved, the observed decay rate, k_{obs} , is given by the Boltzmann relation^{9,61,62} in eq 3, wherein k_{B} is the Boltzmann constant, k_{I} , k_{II} , and k_{III} are the decay rates of the three individual sublevels of the triplet state, and E_{II} and E_{III} are the zero-field splitting (ZFS) energies of the second and third sublevels, respectively, relative to the lowest sublevel. At thermal equilibrium among the three sublevels and in a single, uniform environment, the decay would be single exponential having a decay time constant τ_{obs} according to eq 3. In the present context of nonsingle exponential decay due to local variations of the PMMA host–guest cage, τ_{ave} from the Kohlrausch distribution (eq 2) will be used for τ_{obs} in eq 3 at each temperature.

$$\frac{1}{\tau_{\text{obs}}} = k_{\text{obs}} = \frac{k_{\text{I}} + k_{\text{II}} \exp\left(\frac{-E_{\text{II}}}{k_{\text{B}}T}\right) + k_{\text{III}} \exp\left(\frac{-E_{\text{III}}}{k_{\text{B}}T}\right)}{1 + \exp\left(\frac{-E_{\text{II}}}{k_{\text{B}}T}\right) + \exp\left(\frac{-E_{\text{III}}}{k_{\text{B}}T}\right)} \quad (3)$$

The fact that the average decay time of $[\text{Cp}^*\text{Ir}(\text{piq})(\text{CNAr})][\text{PF}_6]$ was practically constant over the range 77–150 K (Figure 4a) indicates that the three sublevels were thermally populated nearly equally over this temperature range. In all likelihood, this is due to a small ZFS energy relative to $k_{\text{B}}T$ for $[\text{Cp}^*\text{Ir}(\text{piq})(\text{CNAr})][\text{PF}_6]$, as expected for a complex with a highly LC excited state, resulting in a k_{obs} value from eq 3 approaching the limit $k_{\text{T,av}} = (k_{\text{I}} + k_{\text{II}} + k_{\text{III}})/3$. ZFS arises from SOC and is predicted^{9,48,63} to be very small in the absence of much MLCT character. The radiative decay rates also originate from the SOC interaction,^{9,48,63} and the relatively long decay time (32 μs) observed for this temperature range is also characteristic of an emissive state that is highly LC with relatively little MLCT admixture.

Above 150 K, τ_{ave} and β (Figure 4a) decrease precipitously for samples of $[\text{Cp}^*\text{Ir}(\text{piq})(\text{CNAr})][\text{PF}_6]$. The steady-state emission intensity also decreased above 150 K, and with especially rapid drop-off above 200 K (Figure S24). Therefore, the trends to decreasing β and τ_{ave} were attributed to a thermally-activated nonradiative decay.

The nature of the higher lying, nonradiative excited state in $[\text{Cp}^*\text{Ir}(\text{piq})(\text{CNAr})][\text{PF}_6]$ was investigated by fitting eq 4 to the temperature dependence of the observed decay rate, where $k_{\text{T,av}}$ is the observed decay rate for the triplet state in the limit of equal population of the three sublevels ($kT \gg E_{\text{III}}$), k_{a} is the decay rate of the nonradiative state, and E_{a} is the energy for the nonradiative state. Note that eq 4 was obtained by simply adding the Boltzmann terms for the nonradiative state to eq 3. The fit of eq 4 to the data (Figure 5) yields a value of E_{a} as

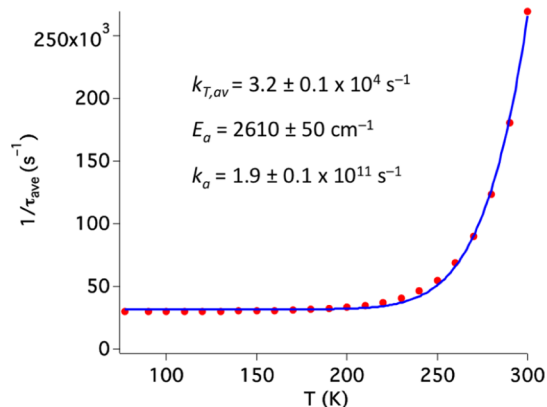


Figure 5. Temperature dependence of the average observed decay rate of $[\text{Cp}^*\text{Ir}(\text{piq})(\text{CNAr})][\text{PF}_6]$ measured in PMMA films. Blue solid curve displays the fit of eq 4 using the values listed.

$2610 \pm 50 \text{ cm}^{-1}$ as an average energy gap between the emissive state and the higher lying state. The value of k_{a} was found to be $1.9 \pm 0.1 \times 10^{11} \text{ s}^{-1}$. A study of temperature dependence of emission decay rate for a large number of Ru(II) and Os(II) diimine complexes⁶⁴ found that the complexes could be grouped into two main types according to the magnitude of the decay rates found for the higher lying state. Those with k_{a} values on the order of 10^{12} to 10^{14} s^{-1} were attributed to d–d states, whereas those with values on the order of 10^7 to 10^8 s^{-1} were attributed to higher lying MLCT states having faster

decay than the lowest energy, emissive state. The value of k_a places the present complex closer to the range where nonradiative decay proceeds via d–d states. The decay rate is somewhat below the expected range,⁶⁴ perhaps because it was doped into the solid PMMA host rather than in solution. The possibility of some participation of a higher lying MLCT state cannot be fully excluded.

$$k_{\text{obs}} = \frac{k_{T,\text{av}} + k_a \exp\left(\frac{-E_a}{k_B T}\right)}{3 + \exp\left(\frac{-E_a}{k_B T}\right)} \quad (4)$$

A decrease in the value of β far from 1 with increasing temperature was similarly reported⁵⁷ for *cis*-[Ru(bpy)₂(py)₂][PF₆]₂ doped into PMMA that also displayed thermally activated nonradiative decay. This was attributed to a dynamical equilibrium between the emissive state and a thermally populated d–d state.⁵⁷ Here, the observation that β is fairly close to 1 for [Cp*Ir(piq)(CNAr)][PF₆] over the lower temperature range suggests that the photophysical properties of the emissive state are only moderately sensitive to local variation in the host–guest cage. From the observation that β decreases so steadily at the higher temperatures, we conclude that the energy of the d–d state and hence its thermal population was strongly affected by the local environment, leading to the widening distribution of decay times at higher temperatures. The effect of varied population of the d–d state upon the distribution of observed decay rates is accentuated because of its fast decay rate relative to that of the emissive state.

Several benchmark complexes were also examined in PMMA to provide support for the hypothesis that the temperature-dependent decrease in the value of β may be attributed to thermal population of a nonradiative state in the inhomogeneous environment. Two Ir(III) complexes known to have very high quantum yields at room temperature⁶⁵ and therefore no thermally populated d–d states were found to exhibit β values close to 1 over the entire range from 77 to 300 K even though the decay times changed substantially (Figures S25 and 26). There was a noticeable trend of smaller β values for [Ru(bpy)₃][PF₆]₂ in PMMA as temperature increased near room temperature (Figure S27), although not nearly to the extent for the above-cited Ru complex⁵⁷ or for [Cp*Ir(piq)(CNAr)][PF₆], both of which have much lower quantum yield because of greater population of the d–d state. As a final reference compound, a Cu(I) complex that displays thermally activated delayed fluorescence⁶⁶ was examined in PMMA (Figure S28). The β value for these decays showed little variation over the temperature range wherein the delayed fluorescence was populated. These results on the benchmark complexes show that some temperature-dependent property of the PMMA alone in the absence of thermal population of nonradiative states does not cause a widening distribution of decays.

The decay time of [Cp*Ir(piq)(NHC)][PF₆] (Figure 4b) exhibits a steady decrease from 4.7 μ s at 77 K to 3.9 μ s at 200 K, with β (Figure 4b) remaining nearly constant and close to 1 (0.97–0.98) over this range. This behavior is in contrast to that of [Cp*Ir(piq)(CNAr)][PF₆], which exhibited decay times that remained relatively constant over a similar range. It is indicative of complexes with a larger ZFS for which the highest sublevel of the emissive triplet state normally has the fastest decay rate and becomes more populated as temperature

increases. A larger ZFS is consistent with the higher MLCT character deduced from the spectroscopic measurements in the previous section, such as the magnitude of $\epsilon(S_0 \rightarrow T_1)$. The shorter decay times observed for [Cp*Ir(piq)(NHC)][PF₆] compared with [Cp*Ir(piq)(CNAr)][PF₆] are also consistent with higher MLCT character for the NHC complex.

As the temperature was increased above 200 K, the decay time of [Cp*Ir(piq)(NHC)][PF₆] shortened distinctly more rapidly. This more rapid decrease in decay time may be attributed to thermal population of a nonradiative state because the steady-state emission decreased dramatically over the same temperature range (Figure S29). The value of β also sharply decreased above 200 K (Figure 4b), correlating with the thermally activated nonradiative decay. Equation 4 cannot be used to determine k_a and E_a for the nonradiative state in this case because the decay rate of the emissive triplet state was not constant with temperature. The ZFS and individual decay rates of the three triplet sublevels would need to be determined to accurately model the temperature dependence of the thermal average decay rate of the emissive state to then be able to determine the k_a and E_a of the nonradiative state from the observed decay temperature dependence. These parameters could in principle be determined from fits of the decay rates to eq 3 at ultra-low temperatures (2–100 K), but this has not been carried out for this complex. For the present survey study, it is only noted that the energy gap E_a for [Cp*Ir(piq)(NHC)][PF₆] must be similar to that in [Cp*Ir(piq)(CNAr)][PF₆] because the temperature range over which the accelerated decrease in emission intensity and decay time occurred is similar.

The decay time of Cp*Ir(piq)(CH₃) in PMMA (Figure 4c) showed a monotonic decrease from 77 to 300 K, not two distinct temperature regimes as for the CNAr and NHC complexes. The parameter β was surprisingly invariable and in a somewhat lower range (0.79–0.85, Figure 4c) compared with that for the previous two compounds. The steady-state emission intensity of Cp*Ir(piq)(CH₃) also showed a steady decline over the whole temperature range (Figure S30). The quantum yield at 77 K in the PMMA host was measured as 0.07 and estimated as 0.01 at 300 K (Table 1). We can only speculate that the relatively small change in β in the presence of thermally activated nonradiative decay is a sign that the thermally populated state does not have so many orders of magnitude faster decay rate than the emissive state and therefore might be a higher lying MLCT state rather than a d–d state. Such a state has been posited as a “4th state” in the temperature-dependent decays in solution of some Ru(II) diimine complexes.^{64,67–69} As a comparison, the thermally activated delayed fluorescence copper complex⁶⁶ (Figure S28) exhibits a fairly constant value of β through the temperature range over which there is an equilibrium between two excited states with decay rates differing by 3 orders of magnitude⁶⁶ not by many more orders of magnitude as is the situation when the thermally populated excited state is a d–d state, as seems to be the case with the CNAr and NHC complexes here.

The bpy complexes that are emissive at room temperature are examined next. The emission decay time of [Cp*Ir(bpy)(CH₃)]₂[PF₆] in PMMA (Figure 6) decreased steadily from 77 to 300 K. The parameter β (Figure 6) also decreased steadily above 77 K, until it leveled off after reaching a low value above about 225 K. The steady-state emission of [Cp*Ir(bpy)(CH₃)]₂[PF₆] also steadily dropped in intensity as the temperature was increased above 77 K (Figure S31). The

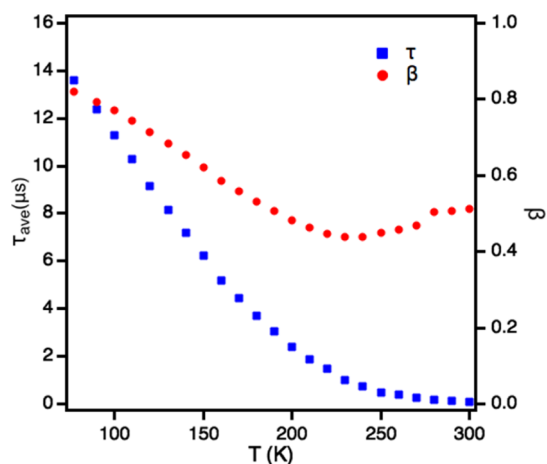


Figure 6. Temperature dependence of average emission decay time constants and the Kohlrausch parameter β of $[\text{Cp}^*\text{Ir}(\text{bpy})(\text{CH}_3)]\text{[PF}_6\text{]}$ measured in PMMA films.

quantum yield measured at 77 K was 0.09 but was extremely low at 300 K (Table 1). Monitoring the emission intensity as the temperature was cycled back down to 77 K showed that the complex was photo-stable in the PMMA matrix, which is noteworthy considering that the photochemical reactivity is observed in solution.³⁴ $[\text{Cp}^*\text{Ir}(\text{bpy})\text{H}][\text{PF}_6]$ in PMMA exhibited similar temperature dependencies for steady-state emission (Figure S32), emission decay time (Figure S33), and Kohlrausch distribution parameter β (Figure S33). The quantum yield was a bit lower at 0.03 at 77 K and extremely low at 300 K (Table 1). Temperature cycling the emission intensity measurement showed that this compound was also photo-stable in the PMMA matrix.

The monotonic decreases in emission intensity, decay time, and parameter β with temperature (i.e., no distinctly different ranges of temperature dependence) for $[\text{Cp}^*\text{Ir}(\text{bpy})(\text{CH}_3)]\text{[PF}_6\text{]}$ and $[\text{Cp}^*\text{Ir}(\text{bpy})\text{H}][\text{PF}_6]$ preclude conclusions on the nature of thermally populated nonradiative state(s) and the energy gap between it and the emissive state. Therefore, a preliminary study of the temperature dependence of the observed decay times at even lower temperatures (1.7–100 K) was carried out in an attempt to freeze out nonradiative states in order that the underlying emissive state temperature dependence could be established according to eq 3. Employing the ZFS and sublevel decay rates thus determined, it might then be possible to determine the energy gap and decay rate of the nonradiative state from the temperature dependence at higher temperatures. For moderate and larger ZFS, the majority population near 2 K will be in the lowest sublevel and the upper sublevels will be frozen out. The emission decay time for both the methyl and the hydride complexes (Figure S34) was longest at the lowest temperature and sharply decreased as the temperature was increased. Group theory models^{70,71} predict that the lowest energy sublevel is the most highly forbidden one, explaining why the decay time is the longest near 2 K. The emission decay time is predicted to shorten as the upper two sublevels are populated as temperature increases, as was observed for the methyl and hydride complexes of the present study. Unfortunately, the Boltzmann-type expression, eq 3, could not be satisfactorily fit to the observed decay times. One possible explanation is that another excited state nearby in energy could be contributing to the observed average decay rates. The number of unknown

parameters that would come with adding terms for an additional state to eq 3 would preclude modeling the temperature dependence with confidence.

Despite the difficulty in fitting the decay temperature dependence to a Boltzmann-type expression, an important qualitative inference may still be drawn from the temperature dependence of the decay rates. A purely MLCT excited state would be expected to have a very large ZFS⁴⁸ and therefore the decay rate would be constant for at least a few degrees above 1.7 K before increasing with the temperature as the higher sublevels were populated. The observation that the decay times for both $[\text{Cp}^*\text{Ir}(\text{bpy})(\text{CH}_3)]\text{[PF}_6\text{]}$ and $[\text{Cp}^*\text{Ir}(\text{bpy})\text{H}][\text{PF}_6]$ increased steadily from 1.7 K indicate that the ZFS, and hence degree of MLCT character, is smaller than that determined for complexes such as *fac*- $\text{Ir}(\text{ppy})_3$ ⁷² and *fac*- $\text{Ir}(\text{piq})_3$ ³⁶ by comparison to the decay temperature dependences reported for the latter two complexes in which there was little change in decay time from about 1.5 K until the temperature was above about 5 K. Yet, the trends in spectroscopic features discussed in the preceding section suggested that the lowest excited states of $[\text{Cp}^*\text{Ir}(\text{bpy})(\text{CH}_3)]^+$ and $[\text{Cp}^*\text{Ir}(\text{bpy})\text{H}]^+$ are highly CT in nature. The nature of the CT state (MLCT vs LLCT) was therefore explored by density functional theory (DFT) predictions of the orbital parentage of the emissive states.

Electronic Structure Calculations. DFT calculations at the B3LYP+D3/LANL2DZ+f,6-311G** level of theory in dichloromethane (SMD) were performed to obtain the optimized ground state (S_0) and lowest triplet excited state (T_1) for $[\text{Cp}^*\text{Ir}(\text{bpy})(\text{CH}_3)]^+$ and $\text{Cp}^*\text{Ir}(\text{piq})(\text{CH}_3)$. The highest occupied molecular orbital (HOMO) and lowest unoccupied molecular orbital (LUMO) at the S_0 geometry and the singly occupied natural orbitals (SONOs) at the T_1 geometry are depicted in Figure 7 for $[\text{Cp}^*\text{Ir}(\text{bpy})(\text{CH}_3)]^+$

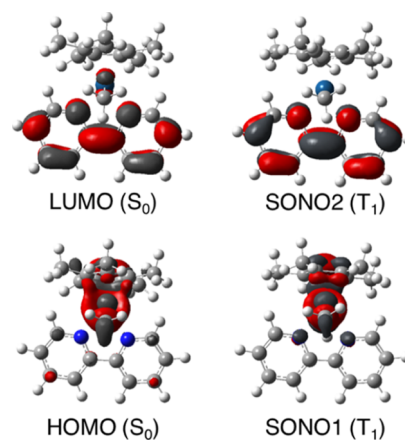


Figure 7. Depictions of the frontier orbitals for $[\text{Cp}^*\text{Ir}(\text{bpy})(\text{CH}_3)]^+$ at the S_0 and at the T_1 optimized geometries.

and in Figure 8 for $\text{Cp}^*\text{Ir}(\text{piq})(\text{CH}_3)$. It may be seen in $[\text{Cp}^*\text{Ir}(\text{bpy})(\text{CH}_3)]^+$ that the LUMO at the S_0 geometry is clearly localized on the bpy ligand, whereas the HOMO is spread over the metal atom and the Cp^* ligand and to a lesser extent on the other ligands. Similarly, for $\text{Cp}^*\text{Ir}(\text{piq})(\text{CH}_3)$, the LUMO appears localized on the piq ligand, whereas the HOMO comprises mainly the metal atom and the Cp^* ligand. For both complexes, the SONOs at the T_1 geometry closely resemble the LUMO and HOMO at S_0 geometry, showing that the T_1 state arises mainly from a HOMO to LUMO transition.

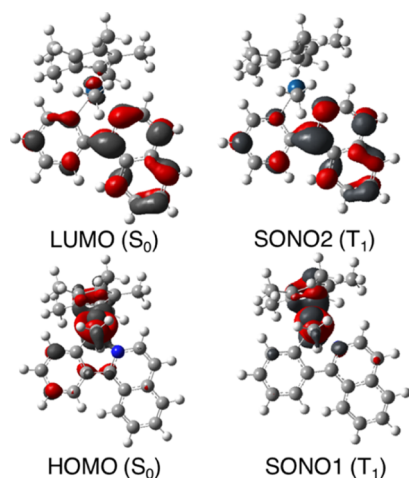


Figure 8. Depictions of the frontier orbitals for $\text{Cp}^*\text{Ir}(\text{piq})(\text{CH}_3)$ at the S_0 and at the T_1 optimized geometries.

Orbital composition analysis for both complexes confirmed that the singly occupied orbitals of T_1 have very similar orbital compositions as the respective HOMOs and LUMOs of S_0 . These results are summarized in Table 3 for $[\text{Cp}^*\text{Ir}(\text{bpy})](\text{CH}_3)]^+$.

Table 3. Orbital Contributions (%) to Frontier MOs for $[\text{Cp}^*\text{Ir}(\text{bpy})](\text{CH}_3)]^+$

atom or group	HOMO (S_0)	LUMO (S_0)	SONO1 (T_1)	SONO2 (T_1)
Ir	37.53	4.18	47.67	1.54
bpy	13.15	92.86	7.07	98.2
Cp^*	35.83	2.18	37.00	0.24
CH_3	13.49	0.78	8.27	0.02

Table 4. Orbital Contributions (%) to Frontier MOs for $\text{Cp}^*\text{Ir}(\text{piq})(\text{CH}_3)$

atom or group	HOMO (S_0)	LUMO (S_0)	SONO1 (T_1)	SONO2 (T_1)
Ir	39.12	3.99	48.20	4.04
piq	23.31	93.50	17.14	93.47
Cp^*	27.48	1.73	28.73	2.05
CH_3	10.08	0.78	5.92	0.44

$(\text{CH}_3)]^+$ and in Table 4 for $\text{Cp}^*\text{Ir}(\text{piq})(\text{CH}_3)$. In particular, 98% of the T_1 SONO2 of $[\text{Cp}^*\text{Ir}(\text{bpy})(\text{CH}_3)]^+$ was found to comprise orbitals from the bpy ligand, whereas the T_1 SONO1 was comprised of very little (7%) from the bpy orbitals but about 48% from the Ir and 37% from the Cp^* group, and a small contribution from the methyl (8%). Calculations reported²⁵ for $[\text{Cp}^*\text{Ir}(\text{bpy})\text{H}]^+$ at the B3LYP/STO-2G,STO-4G level of theory similarly show a highly delocalized HOMO and a LUMO predominantly located on the bpy.

The T_1 excited state is therefore best described as having a predominantly CT character, with very little LC character. This CT character comprises both MLCT and LLCT components, particularly from the Cp^* . Perusal of Table 4 reveals that the T_1 state of $\text{Cp}^*\text{Ir}(\text{piq})(\text{CH}_3)$ has an increased LC character as shown by the 17% piq contribution to SONO1, but that the T_1 is still dominantly of MLCT/LLCT character.

The computational results suggesting that the lowest energy triplet states (T_1) for the above two methyl complexes are

highly CT in nature are experimentally supported by the trends in spectroscopic features discussed earlier. Qualitative experimental support for the more specific description of mixed MLCT + LLCT character was provided by the temperature dependence of decay times (1.7–100 K) for $[\text{Cp}^*\text{Ir}(\text{bpy})(\text{CH}_3)]^+$ that indicated that the ZFS in the emissive state is not larger than that in $\text{Ir}(\text{ppy})_3$ ($E_{\text{II}} = 13.5$ and $E_{\text{III}} = 83 \text{ cm}^{-1}$ in frozen THF),⁷² whereas it would have been predicted to be larger if the MLCT character was much greater.^{9,48,63} Previous TD-DFT calculations⁷¹ on $\text{Ir}(\text{ppy})_3$ at the B3PW91/LANL2DZ,D95 level of theory predicted a majority LC character (58%), whereas the LC content was only 17% in the cyclometalating complex $\text{Cp}^*\text{Ir}(\text{piq})(\text{CH}_3)$. The degree of the MLCT character (40%) in $\text{Ir}(\text{ppy})_3$ was calculated to be similar to that in the two methyl complexes here (about 48%), but the latter additionally have substantial LLCT character. The literature complex $[\text{Ir}(\text{ppy})_2(\text{bpy})]^+$ appears to be much more similar to the present methyl complexes, with calculations at the B3LYP/SBKJC-VDZ,3-21G* level of theory, suggesting 43.7% MLCT character and 51.3% LLCT character and only 5% LC character of the chromophoric bpy ligand in the excited state.¹⁴

DFT calculations were also performed on $[\text{Cp}^*\text{Ir}(\text{piq})(\text{CNAr})]^+$. In this case, the LUMO was found once again to be highly localized on the chromophoric piq ligand, and the HOMO was highly mixed with contributions from Ir and the different ligands (Figure S35). The S_1 state arising from the HOMO to LUMO transition is therefore described as mixed MLCT/LLCT/LC. The T_1 state was found to be very dissimilar (Figure S35), however, and highly LC in character, in agreement with the conclusions drawn from the spectroscopic and photophysical properties. This situation arises when the ^1CT states are relatively close in energy to the ^1LC states. The S–T splitting for LC π – π^* states are generally larger than the S–T splitting for CT states,⁷³ making it possible for the ^3LC to become the lowest excited state. An example of this may be found in a study on $\text{Ir}(\text{ppy})_2(\text{CO})\text{Cl}$, where the S_1 was assigned experimentally as $^1\text{MLCT}$, but the emissive triplet was characterized as highly LC.⁷⁴ The HOMO of the theoretical model complex $[\text{Ir}(\text{tpy})_2(\text{CNCH}_3)]^{2+}$ was calculated to be a mixture of Ir 5d and ligand π orbitals, whereas the LUMO was predominantly ligand π^* ,⁷ corresponding to a mixed MLCT/LC transition. Experimentally, the emissive state of the CN-*t*-Bu analogue was found to be highly ^3LC with relatively small MLCT admixture.⁷

CONCLUSIONS

The ability to change the nature of iridium excited states by installation of strong σ -donor ligands represents a key finding of the present study. In each of the three series of complexes $[\text{Cp}^*\text{Ir}(\text{tpy})\text{L}]^{n+}$, $[\text{Cp}^*\text{Ir}(\text{piq})\text{L}]^{n+}$ ($n = 0$ or 1), and $[\text{Cp}^*\text{Ir}(\text{bpy})\text{L}]^{m+}$ ($m = 1$ or 2), the emission was tuned from highly LC to highly CT in nature just by varying the single ancillary ligand, L. Notably, the present report demonstrates that chemical structures can be designed wherein the electronic environment induces a transition to a C^N-cyclometalating ligand that is very high in CT character. Specifically, the methyl ancillary ligand provided extremely strong σ -donation that induced high CT character transitions to cyclometalating ligands tpy and piq. The high degree of CT character is striking in contrast to other pseudo-octahedral cyclometalated complexes of Ir(III), which normally display emission that is

mainly LC with more moderate admixture of MLCT character. The methyl ancillary ligand also induced high CT character emission in the Cp* complex with the bpy chromophoric ligand, despite the overall cationic charge of the complex and bpy being a relatively weak σ -donor. Thus, these results reveal a new molecular design strategy for producing iridium complexes with high degree of CT character.

Another important finding relates to the orbital parentage of the CT transitions of Cp*Ir-based complexes. Prior studies have focused on the MLCT character of the excited state. DFT calculations on two complexes having methyl ligands reveal that the CT character of the emissive state is not entirely MLCT, however, but includes significant LLCT from the Cp* and a smaller contribution from the methyl ligand in these highly covalent complexes.

The potential impact of strong σ -donor ligands on photocatalysis is exemplified by the H₂ evolution reactivity of [Cp*Ir(bpy)H]⁺ and its analogues. The hydride complex [Cp*Ir(bpy)H]⁺ features spectroscopic and photophysical properties that are remarkably similar to the methyl complex [Cp*Ir(bpy)(CH₃)]⁺, indicating that the hydride and methyl ligands possess similar σ -donor ability. The hydride was previously correctly assigned as having significant MLCT character, although we present evidence that there is in addition significant LLCT character. The importance of the hydride ligand itself in conferring a long-lived triplet excited state was not recognized until the present work, with a focus instead on the role of the bpy ligand. The hydride ligand is obviously a prerequisite for H₂ evolution or hydride transfer reactivity, but the strong σ -donor hydride ligand also confers substantial CT character to the excited state, enabling the productive photochemistry. The CT character also leads to visible light absorption properties that avoid inner filter effects of other Ir species involved in catalysis.⁷⁵ These findings motivate further photophysical investigations of complexes with “reactive” hydride ligands.

EXPERIMENTAL SECTION

Synthesis. The solvents methylene chloride, acetonitrile, THF (unstabilized), and diethyl ether (unstabilized) were stored and dispensed from an MBraun solvent purification system and then stored for use in an MBraun glovebox maintained with a dry N₂ atmosphere. Commercially available reagents were purchased and used as received. Deuterated solvents for NMR spectroscopy were purchased from Cambridge Isotopes. Chemical reactions and manipulations were carried out at room temperature inside the glovebox or using Schlenk techniques. The compounds [Cp*Ir(Cl)(μ -Cl)]₂,⁷⁶ [Cp*Ir(bpy)(NCCH₃)]₂[PF₆]₂,³⁹ [Cp*Ir(bpy)H][PF₆],³⁹ and [Cp*Ir(bpy)(CH₃)]₂[PF₆]₂³⁴ were synthesized according to the cited literature methods. Circulation of the glovebox was stopped while methylene chloride was opened, and the glovebox was purged when finished. ¹H NMR spectra were recorded with a 400 MHz Varian Inova Spectrometer or 600 MHz Bruker spectrometer. ¹³C NMR spectra were recorded as noted either on the Varian operating at 100 MHz or on one of three Bruker Avance spectrometers operating at 125, 150, and 175 MHz, respectively. NMR spectra were processed with the MestReNova software package. High-resolution mass spectrometry (electrospray ionization) was performed at the mass spectrometry facilities at either Michigan State University or at the University of North Carolina, Chapel Hill. Mass spectra at MSU were acquired with a Waters Xevo G2-XS spectrometer with electrospray ionization and TOF-MS detection operating in positive ion mode. Mass spectrometry at UNC-CH was performed on an LTQ FT (ICR 7T) (Thermo Fisher, Bremen, Germany) mass spectrometer. Samples were introduced from acetonitrile solutions via a

microelectrospray source at a flow rate of 3 μ L/min. Xcalibur (ThermoFisher, Bremen, Germany) was used to analyze the data. Molecular formula assignments were determined with Molecular Formula Calculator (v 1.2.3). Elemental analyses were performed by Atlantic Microlab, Norcross, GA. Infrared spectra were recorded on a Bruker Alpha Platinum attenuated total reflectance instrument.

N-formyl-2,6-dimethylaniline. In an adaptation of a general procedure reported previously for the 2,6-diisopropyl analogue,⁷⁷ acetic anhydride (40 mL) was cooled to 0 °C in a 500 mL round-bottom flask and formic acid (20 mL) was added dropwise via a syringe. This solution was warmed under stirring to 50 °C for 2 h and then cooled back to 0 °C. 2,6-Dimethylaniline (5 g, 41.2 mmol) was added via a syringe, and the reaction was allowed to warm to room temperature. After stirring for 1 h, the reaction was cooled to 0 °C and 300 mL of 0 °C water was added, yielding a light pink suspension. The solid product was vacuum-filtered and washed with 1 L of DI water. The solid was dried under vacuum overnight to yield pure product as an off-white solid. Yield: 5.72 g, 93%. ¹H NMR (400 MHz, CDCl₃): Mixture of isomers. δ 8.42 and 8.11–8.08 (s and d, 1H, $-CH=O$), 7.14–7.09 (m, 3H, Ar-H), 6.89 and 6.77 (br s, 1H, $-NH-$), 2.31 and 2.27 (s, 6H, $-CH_3$).

2,6-Dimethylphenylisocyanide. In an adaptation of a general procedure reported previously for the 2,6-diisopropyl analogue,⁷⁷ N-formyl-2,6-dimethylaniline (1 g, 6.70 mmol) was dissolved in 50 mL of dichloromethane in a 250 mL round-bottom flask and cooled to 0 °C. Diisopropylamine (2.5 mL) was added via a syringe, then POCl₃ (0.6 mL) was added dropwise over 20 min. The reaction was allowed to warm to room temperature and stirred for 2 h. A concentrated solution of Na₂CO₃ was added to the reaction mixture, and the biphasic mixture was vigorously stirred overnight. The organic layer was separated, washed with sodium bicarbonate solution, and evaporated. The desired product was purified on a silica column eluted with dichloromethane followed by crystallization from boiling hexanes. Yield: 492 mg, 56%. ¹H NMR (400 MHz, CDCl₃): 7.18 (dd, 1H para Ar-H), 7.10 (d, 2H, meta Ar-H), 2.42 (s, 6H, $-CH_3$). $\nu(C\equiv N)$: 2119 cm⁻¹.

Cp*Ir(2-(*p*-tolyl)pyridinato-N^{Ac}Cl). In a minor modification to the method reported by Li et al.³⁷ for the 2-phenylpyridine analogue, [Cp*Ir(Cl)(μ -Cl)]₂ (303 mg, 0.38 mmol) and NaOAc (178 mg) were placed in a 100 mL round-bottom flask and 10 mL of CH₂Cl₂ was added. 2-(*p*-Tolyl)pyridine (143 μ L, 0.83 mmol) was added by a syringe to the stirring mixture. After about 10 min, the orange [Cp*Ir(Cl)(μ -Cl)]₂ appeared to be taken into the yellow solution stirring with the slurry of excess NaOAc. Stirring was continued overnight. The slurry was filtered and rinsed through celite with additional CH₂Cl₂. The yellow solution was concentrated, layered with diethyl ether, and allowed to stand for 2 h while crystallization began. The product mixture was then refrigerated overnight at -30 °C to promote additional precipitation. Orange powder and crystals were filtered, washed with diethyl ether, and dried under vacuum (354 mg, 87.6% yield). ¹H NMR (400 MHz, CD₂Cl₂): δ : 8.66 (d, J = 5.7 Hz, 1H), 7.79 (d, J = 8.1 Hz, 1H), 7.67 (t, J = 7.7 Hz, 1H), 7.63–7.56 (m, 2H), 7.09 (t, J = 5.9 Hz, 1H), 6.88 (d, J = 7.4 Hz, 1H), 2.43 (s, 1H), 1.67 (s, 15H). ¹³C NMR (101 MHz, CD₂Cl₂): δ 167.44, 163.94, 151.68, 142.25, 140.90, 137.36, 136.85, 123.88, 123.33, 122.30, 118.81, 88.83, 21.79, 9.02. HRMS (ESI⁺) m/z : [M – Cl]⁺ found (theory) for C₂₂H₂₅NiIr, 496.1620 (496.1617). Anal. found (calcd) for C₂₂H₂₅NiIrCl: C, 49.89 (49.75); H, 4.72 (4.74); N 2.65 (2.64).

[Cp*Ir(2-(*p*-tolyl)pyridinato-N^{Ac})(NCCH₃)]₂[PF₆]. Cp*Ir(2-(*p*-tolyl)pyridinato-N^{Ac}Cl) (194 mg, 0.365 mmol) was placed in a 100 mL round-bottom flask and partly dissolved with CH₃CN (6 mL). AgPF₆ (97 mg, 0.384 mmol) was dissolved in CH₃CN (2 mL) and added dropwise to the stirring slurry of Cp*Ir(2-(*p*-tolyl)pyridinato-N^{Ac}Cl). A white precipitate appeared, and the remaining orange crystals of Cp*Ir(2-(*p*-tolyl)pyridinato-N^{Ac}Cl) were gradually taken into solution. Stirring was continued for an additional 2 h. The mixture was filtered through celite, and the pale yellow solution was

concentrated. The product solution was layered with diethyl ether and allowed to stand for 5 h to begin crystallization, and then refrigerated at $-30\text{ }^{\circ}\text{C}$ overnight. Light yellow crystals were filtered, washed lightly with diethyl ether, and allowed to dry in the glovebox atmosphere (193 mg, 77.5% yield). The product was not subject to drying under vacuum as a precaution against loss of potentially fugitive CH_3CN ligand. This intermediate compound was used promptly without further purification for subsequent synthesis.

[Cp*Ir(2-(*p*-tolyl)pyridinato- $\text{N}^{\wedge}\text{C}^2$ ')(2,6-dimethylphenylisocyanide)][PF₆]. [Cp*Ir(2-(*p*-tolyl)pyridinato- $\text{N}^{\wedge}\text{C}^2$ ')(NCCH₃)] [PF₆] (85 mg, 0.125 mmol) was dissolved in 5 mL of CH_3CN in a 50 mL round-bottom flask. 2,6-Dimethylphenylisocyanide (25 mg, 0.191 mmol) was added as a solid to the reaction flask and quickly dissolved. Stirring was continued overnight. The reaction solution was concentrated, layered with diethyl ether, and refrigerated overnight at $-30\text{ }^{\circ}\text{C}$. Pale yellow crystals and powder were filtered, washed with diethyl ether, and dried (85 mg, 84% yield). ¹H NMR (400 MHz, CD₂Cl₂): δ 8.58 (d, *J* = 5.9 Hz, 1H), 7.93 (d, *J* = 3.8 Hz, 2H), 7.69 (d, *J* = 8.0 Hz, 1H), 7.46 (s, 1H), 7.31–7.23 (m, 1H), 7.16–7.07 (m, 2H), 7.02 (d, *J* = 7.6 Hz, 2H). ¹³C NMR (176 MHz, CD₂Cl₂): δ 167.80, 153.24, 150.01, 142.73, 142.27, 140.00, 137.37, 135.19, 129.62, 129.41, 128.28, 127.26, 126.01, 125.30, 123.90, 120.45, 97.57, 21.67, 18.20, 9.25. HRMS (ESI⁺) *m/z*: [M – PF₆]⁺ found (theory) for C₃₁H₃₄N₂Ir, 627.2355 (627.2353). Anal. found (calcd) for C₃₁H₃₄N₂IrPF₆: C, 48.05 (48.24); H, 4.48 (4.44); N 3.53 (3.63). $\nu(\text{C}\equiv\text{N})$: 2149 cm⁻¹.

[Cp*Ir(2-(*p*-tolyl)pyridinato- $\text{N}^{\wedge}\text{C}^2$ ')(3,5-dimethylimidazol-2-ylidene)][PF₆]. [Cp*Ir(2-(*p*-tolyl)pyridinato- $\text{N}^{\wedge}\text{C}^2$ ')(NCCH₃)] [PF₆] (111 mg, 0.163 mmol), 1,3-dimethylimidazolium iodide (38 mg, 0.170 mmol), and Ag₂O (21 mg, 0.0906 mmol) were combined in a glass reaction tube. CH₂Cl₂ was added, and stirring in the dark was continued overnight. The mixture was filtered through celite, and the pale yellow solution was concentrated to about 2 mL. An approximately equal volume of THF was added while stirring. The mixture was layered with diethyl ether and allowed to stand for 2 h during which time precipitation began. The mixture was refrigerated at $-30\text{ }^{\circ}\text{C}$ overnight. Yellow powder was filtered, washed with diethyl ether, and dried (88 mg, 73.4% yield). A second crop of 9 mg was obtained by concentrating the supernatant to dryness, redissolving in a minimal amount of THF and layering with diethyl ether to precipitate. ¹H NMR (400 MHz, CD₂Cl₂): δ 8.74 (d, *J* = 5.9 Hz, 1H), 7.74–7.76 (m, 3H), 7.52 (d, *J* = 7.9 Hz, 1H), 7.20–7.12 (m, 1H), 6.96 (d, *J* = 7.9 Hz, 1H), 6.77 (s, 2H), 3.44 (s, 6H), 2.46 (s, 3H), 1.73 (s, 15H). ¹³C NMR (101 MHz, CD₂Cl₂): δ 173.07, 169.01, 156.72, 153.74, 147.10, 143.32, 140.03, 139.24, 138.70, 125.10, 124.32, 124.29, 121.96, 119.84, 92.93, 39.24, 21.95, 9.17. HRMS (ESI⁺) *m/z*: [M – PF₆]⁺ found (theory) for C₂₇H₃₃N₃Ir, 592.2313 (592.2305). Anal. found (calcd) for C₂₇H₃₃N₃IrPF₆: C, 43.73 (44.02); H, 4.44 (4.51); N 5.56 (5.70).

Cp*Ir(2-(*p*-tolyl)pyridinato- $\text{N}^{\wedge}\text{C}^2$ ')(CH₃). In a minor modification to the method reported by Park-Gehrke et al.³⁸ for the 2-phenylpyridine analog, a 50 mL Schlenk flask was charged with Cp*Ir(tpy)Cl (39.1 mg, 0.074 mmol), 20 mL of THF, and a stir bar inside an N₂ glovebox. The flask was sealed with a septum, brought out of the glovebox, and cooled to $-78\text{ }^{\circ}\text{C}$, and 150 μL methyl lithium solution (1.6 M in Et₂O, 0.24 mmol, 3.2 equiv) was added by syringe. The reaction was allowed to warm to room temperature over which the solution darkened from yellow to a reddish-brown. The solvent was removed in vacuo, and the product was extracted with 2 \times 20 mL of pentane and filtered under N₂ to separate remaining salts. The air-stable filtrate was dried by rotary evaporation. Layering water under a solution of the product in CH₃CN at 4 $^{\circ}\text{C}$ produced bright red crystals (17.6 mg, 0.034 mmol, 47% yield). ¹H NMR (600 MHz, CDCl₃): δ 8.45 (d, *J* = 5.9 Hz, 1H), 7.77 (d, *J* = 8.1 Hz, 1H), 7.65 (d, *J* = 7.8 Hz, 1H), 7.50 (ddd, *J* = 8.4, 7.3, 1.5 Hz, 1H), 7.42 (s, 1H), 6.85 (dd, *J* = 7.9, 1.7 Hz, 1H), 6.81 (ddd, *J* = 7.3, 5.7, 1.4 Hz, 1H), 2.46 (s, 3H), 1.77 (s, 15H, Cp*), -0.28 (s, 3H, IrCH₃). ¹³C NMR (151 MHz, CDCl₃): δ 169.37, 166.63, 150.67, 140.36, 139.19, 135.46,

133.89, 124.02, 120.85, 120.49, 118.55, 88.95, 21.97, 8.88, -15.95 . HRMS (ESI⁺) *m/z*: [M]⁺ found (theory) for C₂₃H₂₈NiIr, 511.1855 (511.1852); [M – CH₃]⁺ found (theory) for C₂₂H₂₅NiIr, 496.1628 (496.1617). Anal. found (calcd) for C₂₃H₂₈NiIr: C, 54.16 (54.09); H, 5.41 (5.53); N 2.93 (2.74).

Cp*Ir(1-phenylisoquinolino- $\text{N}^{\wedge}\text{C}^2$)Cl. In a minor modification to the method reported by Li et al.³⁷ for the 2-phenylpyridine analog, [Cp*Ir(Cl)(μ -Cl)]₂ (357 mg, 0.448 mmol), 1-phenylisoquinoline (202 mg, 0.984 mmol), and NaOAc (210 mg) were placed in a 100 mL round-bottom flask, and 20 mL of CH₂Cl₂ was added. After stirring about 10 min, the orange solution began to turn red and the remaining [Cp*Ir(Cl)(μ -Cl)]₂ appeared to be taken into solution. Stirring was continued overnight. The slurry was filtered and rinsed through celite with additional CH₂Cl₂. The red solution was concentrated, layered with diethyl ether, and allowed to stand for 2 h while crystallization began. The product mixture was then refrigerated overnight at $-30\text{ }^{\circ}\text{C}$ to promote additional precipitation. The resulting red crystals were filtered, washed with diethyl ether, and dried under vacuum (465 mg, 91.5% yield). ¹H NMR (400 MHz, CD₂Cl₂): δ 8.95–8.89 (m, 1H), 8.59 (d, *J* = 6.3 Hz, 1H), 8.30 (d, *J* = 8.1 Hz, 1H), 7.92 (d, *J* = 6.3 Hz, 2H), 7.76–7.69 (m, 2H), 7.46 (d, *J* = 6.3 Hz, 1H), 7.21 (t, *J* = 7.5 Hz, 1H), 7.13 (t, *J* = 7.3 Hz, 1H), 1.67 (s, 15H). ¹³C NMR (176 MHz, CD₂Cl₂): δ 168.28, 167.89, 146.18, 144.92, 137.47, 137.02, 131.36, 130.90, 130.07, 128.40, 127.68, 127.26, 126.53, 122.18, 121.20, 89.57, 9.27.

HRMS (ESI⁺) *m/z*: [M – Cl]⁺ found (theory) for C₂₅H₂₅NiIr, 532.1621 (532.1617). Anal. found (calcd) for C₂₅H₂₅NiIrCl: C, 52.90 (52.94); H, 4.45 (4.44); N 2.48 (2.47).

[Cp*Ir(1-phenylisoquinolino- $\text{N}^{\wedge}\text{C}^2$ ')(NCCH₃)] [PF₆]. Cp*Ir(1-phenylisoquinolino- $\text{N}^{\wedge}\text{C}^2$)Cl (303 mg, 0.534 mmol) was placed in a 100 mL round-bottom flask and partly dissolved with CH₃CN (4 mL). AgPF₆ (150 mg, 0.593 mmol) was dissolved in CH₃CN (2 mL) and added dropwise to the stirring reaction mixture of Cp*Ir(1-phenylisoquinolino- $\text{N}^{\wedge}\text{C}^2$)Cl. A white precipitate appeared as the remaining red crystals of Cp*Ir(1-phenylisoquinolino- $\text{N}^{\wedge}\text{C}^2$)Cl were gradually taken into solution. Stirring was continued an additional 2 h. The mixture was filtered through celite, and the orange solution was concentrated. The product solution was layered with diethyl ether and allowed to stand for 2 h to begin crystallization, and then refrigerated at $-30\text{ }^{\circ}\text{C}$ overnight. The resulting orange crystals were filtered, washed lightly with diethyl ether, and allowed to dry in the glovebox atmosphere (346 mg, 90.2% yield). The product was not subject to drying under vacuum as a precaution against loss of potentially fugitive CH₃CN ligand. This intermediate compound was used promptly without further purification for further synthesis.

[Cp*Ir(1-phenylisoquinolino- $\text{N}^{\wedge}\text{C}^2$ ')(2,6-dimethylphenylisocyanide)] [PF₆]. Diethyl Ether. [Cp*Ir(1-phenylisoquinolino- $\text{N}^{\wedge}\text{C}^2$ ')(NCCH₃)] [PF₆] (60 mg, 0.0836 mmol) was dissolved in 1 mL of CH₂Cl₂ in a 50 mL round-bottom flask. 2,6-Dimethylphenylisocyanide (13 mg, 0.0991 mmol) was dissolved in 1 mL of CH₂Cl₂ and added dropwise to the stirring reaction solution. Stirring was continued for 4 h. The reaction solution was layered with diethyl ether and let stand 5 h at room temperature. A pale orange precipitate formed and was washed with diethyl ether and dried (48 mg, 71.1% yield). ¹H NMR (400 MHz, CD₂Cl₂): δ 8.95 (d, *J* = 8.3 Hz, 1H), 8.47 (d, *J* = 6.4 Hz, 1H), 8.41 (d, *J* = 7.2 Hz, 1H), 8.05 (d, *J* = 7.2 Hz, 1H), 7.92–7.84 (m, 2H), 7.83–7.79 (m, 1H), 7.63 (d, *J* = 6.5 Hz, 4H), 7.41–7.31 (m, 2H), 7.14–7.07 (m, 1H), 7.00 (d, *J* = 7.6 Hz, 2H), 1.94 (s, 6H), 1.91 (s, 15H). ¹³C NMR (176 MHz, CD₂Cl₂): δ 168.61, 153.15, 146.36, 145.18, 137.91, 137.47, 135.25, 132.87, 131.95, 131.35, 129.69, 129.48, 128.27, 128.12, 127.24, 126.88, 126.66, 124.88, 122.79, 97.94, 18.32, 9.35. HRMS (ESI⁺) *m/z*: [M – PF₆]⁺ found (theory) for C₃₄H₃₄N₂Ir, 663.2356 (663.2353). Anal. found (calcd) for C₃₄H₃₄N₂IrPF₆: C, 51.42 (51.75); H, 4.75 (5.02); N 3.15 (3.11). $\nu(\text{C}\equiv\text{N})$: 2140 cm⁻¹.

[Cp*Ir(1-phenylisoquinolino- $\text{N}^{\wedge}\text{C}^2$ ')(3,5-dimethylimidazol-2-ylidene)] [PF₆]. [Cp*Ir(1-phenylisoquinolino- $\text{N}^{\wedge}\text{C}^2$)

(NCCCH_3)] $[\text{PF}_6]$ (113 mg, 0.157 mmol), 1,3-dimethylimidazolium iodide (37 mg, 0.165 mmol), and Ag_2O (20 mg, 0.0863 mmol) were combined in a glass reaction tube. CH_2Cl_2 was added, and the resulting solution was dark red. The mixture was stirred in the dark overnight and filtered through celite, and the solvent was removed. The crude orange product was dissolved in 3 mL of THF, and diethyl ether was added to precipitate the product (110 mg, 90.4% yield). Recrystallization removed some retained THF. ^1H NMR (400 MHz, CD_2Cl_2): δ 8.69 (d, $J = 8.4$ Hz, 1H), 8.56 (d, $J = 6.5$ Hz, 1H), 8.22 (d, $J = 8.0$ Hz, 1H), 8.12 (d, $J = 7.6$ Hz, 1H), 7.97 (d, $J = 8.4$ Hz, 1H), 7.82–7.67 (m, 2H), 7.49 (d, $J = 6.4$ Hz, 1H), 7.29–7.16 (m, 2H), 6.73 (s, 2H), 3.37 (s, 6H), 1.78 (s, 15H). ^{13}C NMR (176 MHz, CD_2Cl_2): δ 169.18, 159.05, 147.59, 146.49, 145.35, 138.72, 137.18, 132.05, 131.14, 129.59, 128.59, 127.43, 127.21, 126.12, 124.07, 122.65, 119.48, 93.58, 39.09, 9.05. HRMS (ESI⁺) m/z : $[\text{M} - \text{PF}_6]^+$ found (theory) for $\text{C}_{30}\text{H}_{33}\text{N}_3\text{Ir}$, 628.2303 (628.2305). Anal. found (calcd) $\text{C}_{30}\text{H}_{33}\text{N}_3\text{IrPF}_6$: C, 46.78 (46.63); H, 4.27 (4.30); N 5.41 (5.44).

$\text{Cp}^*\text{Ir}(\text{1-phenylisoquinolinato-N}^{\text{Ac}^2})(\text{CH}_3)$. In a modification to the method reported by Park-Gehrke et al.³⁸ for the 2-phenylpyridine analog, a 500 mL Schlenk flask was charged with $\text{Cp}^*\text{Ir}(\text{piq})\text{Cl}$ (235.0 mg, 0.414 mmol) and a stir bar. Dry, degassed THF (300 mL) was transferred to the Schlenk flask via cannula. After $\text{Cp}^*\text{Ir}(\text{piq})\text{Cl}$ fully dissolved, the solution was cooled to -78 °C and 2.4 mL of CH_3MgBr solution (3 M in ether, 7.2 mmol) was added by syringe. The stirring solution was allowed to come to room temperature over the course of 3 h, during which time the solution darkened to a wine red. The THF was evaporated in vacuo, and the product extracted into pentane and dried. The resulting air-sensitive solid was rinsed with water and recrystallized by layering water under the product in CH_3CN , resulting in dark red crystals of $\text{Cp}^*\text{Ir}(\text{piq})(\text{CH}_3)$ (109.4 mg, 0.200 mmol, 48% yield). ^1H NMR (600 MHz, CD_2Cl_2): δ 8.94 (d, $J = 8.3$ Hz, 1H), 8.42 (d, $J = 8.1$ Hz, 1H), 8.37 (d, $J = 6.5$ Hz, 1H), 7.83 (d, $J = 7.7$ Hz, 1H), 7.76–7.73 (m, 1H), 7.67–7.59 (m, 2H), 7.16 (d, $J = 6.5$ Hz, 1H), 7.07 (ddt, $J = 9.1, 7.0, 3.7$ Hz, 2H), 1.77 (s, 15H), -0.34 (s, 3H). ^{13}C NMR (151 MHz, CD_2Cl_2): δ 173.67, 164.89, 145.09, 144.25, 135.82, 135.55, 130.00, 129.59, 128.92, 127.65, 127.57, 127.29, 126.39, 119.21, 119.14, 90.23, 8.85, -15.08 . $\lambda_{\text{max}} = 277$ nm ($19\,800\text{ M}^{-1}\text{ cm}^{-1}$), 329 nm ($14\,100\text{ M}^{-1}\text{ cm}^{-1}$), 472 nm ($7500\text{ M}^{-1}\text{ cm}^{-1}$). HRMS (ESI⁺) m/z : $[\text{M} - \text{CH}_3]^+$ calcd for $\text{C}_{25}\text{H}_{25}\text{IrN}$, 532.1616; found 532.16261. Anal. found (calcd) for $\text{C}_{26}\text{H}_{28}\text{IrN}$: C, 57.12 (56.89); H, 5.16 (5.14); N, 2.56 (2.57).

$[\text{Cp}^*\text{Ir}(\text{2,2'-bipyridine})(\text{2,6-dimethylphenylisocyanide})][\text{PF}_6]_2$. $[\text{Cp}^*\text{Ir}(\text{bpy})(\text{NCCCH}_3)]_2[\text{PF}_6]_2$ (83 mg, 0.102 mmol) was placed in a 50 mL round-bottom flask and dissolved in 3 mL of CH_3CN . 2,6-Dimethylphenylisocyanide (20 mg, 0.152 mmol) was added as a solid to the stirring reaction solution and chased with an additional 2 mL of CH_3CN . Stirring was continued 5 h. The reaction solution was layered with diethyl ether, resulting in a very pale yellow precipitate. The crude product was filtered, washed with diethyl ether, and dried (71 mg). Because the NMR showed a small amount of unreacted starting material, the crude product was redissolved in 3 mL of CH_3CN and an additional 2,6-dimethylphenylisocyanide (5 mg) was added. The mixture was stirred for 3 h before layering once again with diethyl ether. The resulting pale yellow needles were filtered, washed, and dried (51 mg). A second crop of 11 mg was obtained for a total yield of 67.3%. ^1H NMR (400 MHz, CD_2Cl_2): δ 8.97 (d, $J = 4.9$ Hz, 2H), 8.52 (d, $J = 7.5$ Hz, 2H), 8.43–8.35 (m, 2H), 8.04–7.98 (m, 2H), 7.29–7.21 (m, 1H), 7.10 (d, $J = 7.8$ Hz, 2H), 2.04 (s, 6H), 1.94 (s, 15H). ^{13}C NMR (176 MHz, CD_3CN): δ 157.38, 154.42, 143.05, 136.82, 131.72, 130.84, 129.14, 126.47, 99.60, 18.38, 9.15. HRMS (ESI⁺) m/z : $[\text{M} - \text{PF}_6]^+$ found (theory) for $\text{C}_{29}\text{H}_{32}\text{N}_3\text{PF}_6\text{Ir}$, 760.1876 (760.1868). Anal. found (calcd) for $\text{C}_{29}\text{H}_{32}\text{N}_3\text{P}_2\text{F}_{12}\text{Ir}$: C, 38.52 (38.50); H, 3.50 (3.57); N 4.73 (4.64). $\nu(\text{C}\equiv\text{N})$: 2173 cm^{-1} .

$\text{Cp}^*\text{Ir}(\text{3,5-dimethylimidazol-2-ylidene})\text{Cl}_2$. The reported procedure⁴⁰ for this complex was modified to combine all reagents in one flask and carry out the reaction in one step. $[\text{Cp}^*\text{Ir}(\text{Cl})(\mu\text{-Cl})_2]$ (267 mg, 0.335 mmol), 1,3-dimethylimidazolium iodide (165 mg, 0.737

mmol), Ag_2O (85 mg, 0.369 mmol) were combined in a reaction tube with 10 mL of CH_2Cl_2 . The tube was wrapped in foil to protect from light and stirred overnight. The resultant orange solution was filtered from off-white precipitate through celite. The solvent was removed, and the orange solid was triturated with THF in which it was sparingly soluble and then filtered. The crude product was redissolved in CH_2Cl_2 and layered with THF. After standing for 2 h, the layered mixture was refrigerated at -30 °C overnight. The orange crystals that formed were filtered, washed with a very small amount of THF, then diethyl ether, and dried (222 mg, 67.0% yield). ^1H NMR (400 MHz, CD_2Cl_2): δ 6.96 (s, 2H), 3.92 (s, 6H), 1.58 (s, 15H). HRMS (ESI⁺) m/z : $[\text{M} - \text{Cl}]^+$ found (theory) for $\text{C}_{15}\text{H}_{23}\text{N}_2\text{IrCl}$, 459.1173 (459.1171). Anal. found (calcd) for $\text{C}_{15}\text{H}_{23}\text{N}_2\text{IrCl}_2$: C, 36.38 (36.44); H, 4.90 (4.69); N 5.68 (5.67).

$[\text{Cp}^*\text{Ir}(\text{3,5-dimethylimidazol-2-ylidene})(\text{NCCCH}_3)_2][\text{CF}_3\text{SO}_3]_2$. A 100 mL round-bottom flask was charged with $\text{Cp}^*\text{Ir}(\text{3,5-dimethylimidazol-2-ylidene})\text{Cl}_2$ (91 mg, 0.184 mmol) and 5 mL of CH_3CN . Silver triflate (102 mg, 0.397 mmol) was dissolved in 2 mL of CH_3CN and added dropwise to the stirring reaction solution. A white precipitate soon appeared and stirring was continued for 2 h as the solution turned pale yellow. The reaction mixture was filtered through celite, concentrated, and filtered once more through a syringe filter. The pale yellow solution was layered with diethyl ether, and a pale yellow oil soon formed. The oil was triturated with diethyl ether until it solidified. The product was not subject to drying under vacuum as a precaution against loss of potentially fugitive CH_3CN ligand. This intermediate compound was used promptly without further purification for further synthesis.

$[\text{Cp}^*\text{Ir}(\text{bpy})(\text{3,5-dimethylimidazol-2-ylidene})][\text{CF}_3\text{SO}_3]_2$. $[\text{Cp}^*\text{Ir}(\text{3,5-dimethylimidazol-2-ylidene})(\text{NCCCH}_3)_2][\text{CF}_3\text{SO}_3]_2$ (92 mg, 0.115 mmol) was placed in a 50 mL round-bottom flask and partly dissolved in 5 mL of THF. 2,2'-Bipyridine (27 mg, 0.173 mmol) was dissolved in 5 mL of THF and added dropwise to the stirring reaction mixture. The starting material was not readily taken into solution, but after stirring overnight, there was a yellow precipitate and nearly colorless supernatant. The crude product was filtered, then redissolved in minimal CH_3CN (1 mL), and passed through a syringe filter. THF (5 mL) was added, and then the mixture was layered with diethyl ether. After standing overnight, the resulting yellow crystals were filtered, washed with diethyl ether, and dried (80 mg, 79.6% yield). ^1H NMR (400 MHz, CD_2Cl_2): δ 9.38 (d, $J = 5.0$ Hz, 2H), 8.38 (d, $J = 7.0$ Hz, 2H), 8.27 (t, $J = 6.0$ Hz, 2H), 8.11 (t, $J = 6.0$ Hz, 2H), 6.94 (s, 2H), 3.47 (s, 6H), 1.78 (s, 15H). ^{13}C NMR (176 MHz, CD_3CN): δ 158.17, 154.98, 145.67, 141.82, 128.93, 126.10, 125.89, 122.08 (CF_3SO_3^- , $q, J = 321$ Hz), 94.80, 39.14, 8.78. HRMS (ESI⁺) m/z : $[\text{M} - \text{CF}_3\text{SO}_3]^+$ found (theory) for $\text{C}_{26}\text{H}_{31}\text{N}_4\text{O}_3\text{SF}_3\text{Ir}$, 729.1695 (729.1697). Anal. found (calcd) for $\text{C}_{27}\text{H}_{31}\text{N}_4\text{O}_6\text{S}_2\text{F}_6\text{Ir}$: C, 36.78 (36.94); H, 3.47 (3.56); N, 6.20 (6.38).

Photophysical Measurements. Optical absorption spectra were recorded in spectrophotometric grade solvents with a Shimadzu UV-3600 spectrophotometer. PMMA samples were prepared by first dissolving a quantity of the phosphors in methylene chloride, and then slowly adding an amount of PMMA to make the concentration of the phosphor to 0.5% by weight with respect to the PMMA. Because the $[\text{Cp}^*\text{Ir}(\text{bpy})\text{H}][\text{PF}_6]$ was unstable in methylene chloride, an amount of PMMA was first dissolved in THF by soaking overnight, and then the appropriate amount of the phosphor was added and dissolved by mixing. The phosphor/PMMA solutions were then transferred to molds of polyethylene vial caps that were placed in a flat-bottom Erlenmeyer flask having a ground glass joint. A T-shaped adapter with entry and exit stopcocks was attached, and a steady stream of nitrogen was passed through the apparatus to dry the doped PMMA samples. These could then be freed by cutting away the polyethylene molds in air and mounted in the cryostats. Steady-state emission spectra from 77 to 300 K were obtained using an Oxford Instruments Optistat DN cryostat with an Edinburgh Instruments FS920 fluorimeter that was equipped with a 450 W Xe arc lamp for excitation source and a Peltier-cooled Hamamatsu R2658P photomultiplier tube (PMT). The Oxford cryostat was also used with an Edinburgh Instruments LP920 laser flash photolysis system

for which a tunable Vibrant 355 nm Nd/YAG/OPO system (Opotek) was the excitation source and a Hamamatsu R928 PMT was the detector. For emission measurements in the temperature range of 1.7–100 K, a liquid helium cryostat (Cryovac Konti Cryostat IT) was used in conjunction with a Horiba Jobin Yvon Fluorolog 3 steady-state fluorescence fluorimeter that was modified to additionally enable measurements of emission decay times. As excitation source with the liquid helium cryostat, a PicoQuant LDH-P-C-375 pulsed diode laser ($\lambda_{\text{exc}} = 372$ nm, pulse width 100 ps) was used. The emission signal was detected with a cooled photomultiplier attached to a FAST ComTec multichannel scalar PCI card with a time resolution of 250 ps. Absolute photoluminescence quantum yields were determined with a Hamamatsu C9920-02 system equipped with a Spectralon integrating sphere.

DFT calculations. DFT calculations were performed using Gaussian 09.⁷⁸ All complexes were optimized in their singlet and triplet states using the B3LYP functional^{79,80} with the Grimme's D3 dispersion correction.⁸¹ The LANL2DZ⁸² basis set and accompanying pseudopotential with an additional f polarization function⁸³ were used for the iridium center, and 6-311G** basis set^{84,85} was used for all other atoms. Frequency calculations were performed on all optimized structures to verify the nature of stationary points, and no imaginary frequencies were obtained. Natural orbital analysis was used to analyze the electronic structure of the optimized triplet states. The SMD solvation model⁸⁶ (dichloromethane solvent) was employed for all calculations. Multiwfn software⁸⁷ was utilized to perform Mulliken population analysis to quantify frontier molecular orbital compositions.

■ ASSOCIATED CONTENT

● Supporting Information

The Supporting Information is available free of charge on the ACS Publications website at DOI: [10.1021/acs.inorgchem.8b02753](https://doi.org/10.1021/acs.inorgchem.8b02753).

¹H and ¹³C NMR spectra; additional absorption and photoluminescence spectra; temperature dependence of emission spectra; additional temperature dependence of photoluminescence decay time constant and parameter β (77–300 K); temperature dependence of photoluminescence decay time constant (1.7–100 K); frontier orbitals of [Cp*Ir(piq)(CNAr)]⁺; and the 3D structures (XYZ) of [Cp*Ir(bpy)(CH₃)]⁺, Cp*Ir(piq)(CH₃), and [Cp*Ir(piq)(CNAr)]⁺ (PDF)

■ AUTHOR INFORMATION

Corresponding Authors

*E-mail: jcdeaton@ncsu.edu (J.C.D.).

*E-mail: ajmm@email.unc.edu (A.J.M.M.).

*E-mail: fncastel@ncsu.edu (F.N.C.).

ORCID

Catherine L. Pitman: 0000-0003-2094-8280

Elena Jakubikova: 0000-0001-7124-8300

Alexander J. M. Miller: 0000-0001-9390-3951

Felix N. Castellano: 0000-0001-7546-8618

Present Address

^{||}Surface Chemistry Branch (Code 6170), U. S. Naval Research Laboratory, Washington, D.C. 20375, United States.

Notes

The authors declare no competing financial interest.

■ ACKNOWLEDGMENTS

This work was supported by the U.S. Department of Energy, Office of Science, Office of Basic Energy Sciences, under Award nos. DE-SC0014255 (synthesis and structural charac-

terization) and DE-SC0011979 (synthesis and structural characterization, static and time-resolved spectroscopy, and computational studies). We also acknowledge the use of the computing resources of the High-Performance Computing Center at NCSU. C.L.P. was a Fellow of the Royster Society at UNC Chapel Hill. R.C. thanks the European Research Council (ERC) (project no. 645628 “METCOPH”) and the Deutsche Forschungsgemeinschaft (grant no. 389797483) for support. The authors are deeply grateful to Prof. Dr. Hartmut Yersin, Universität Regensburg, for permitting the use of his laboratory for the photoluminescence measurements between 1.7 and 80 K and the absolute quantum yield experiments. We thank Alexander Schinabeck from Regensburg for technical assistance. We thank Joseph Favale, North Carolina State University, for the synthesis of the 2,6-dimethylphenylisocyanide ligand.

■ REFERENCES

- (1) Sprouse, S.; King, K. A.; Spellane, P. J.; Watts, R. J. Photophysical effects of metal-carbon sigma bonds in ortho-metalated complexes of iridium(III) and rhodium(III). *J. Am. Chem. Soc.* **1984**, *106*, 6647–6653.
- (2) Watts, R. J. Photogeneration of Strong One- and Two-Electron Redox Agents from Transition Metal Complexes. *Comments Inorg. Chem.* **1991**, *11*, 303–337.
- (3) King, K. A.; Spellane, P. J.; Watts, R. J. Excited-State Properties of a Triply Ortho-Metalated Iridium(III) Complex. *J. Am. Chem. Soc.* **1985**, *107*, 1431–1432.
- (4) Colombo, M. G.; Brunold, T. C.; Riedener, T.; Guedel, H. U.; Fortsch, H.-B. Facial tris cyclometalated rhodium(3+) and iridium(3+) complexes: their synthesis, structure, and optical spectroscopic properties. *Inorg. Chem.* **1994**, *33*, 545–550.
- (5) Hofbeck, T.; Yersin, H. The Triplet State of *fac*-Ir(ppy)₃. *Inorg. Chem.* **2010**, *49*, 9290–9299.
- (6) Sajoto, T.; Djurovich, P. I.; Tamayo, A. B.; Oxgaard, J.; Goddard, W. A., III; Thompson, M. E. Temperature Dependence of Blue Phosphorescent Cyclometalated Ir(III) Complexes. *J. Am. Chem. Soc.* **2009**, *131*, 9813–9822.
- (7) Li, J.; Djurovich, P. I.; Alleyne, B. D.; Yousufuddin, M.; Ho, N. N.; Thomas, J. C.; Peters, J. C.; Bau, R.; Thompson, M. E. Synthetic Control of Excited-State Properties in Cyclometalated Ir(III) Complexes Using Ancillary Ligands. *Inorg. Chem.* **2005**, *44*, 1713–1727.
- (8) Rausch, A. F.; Homeier, H. H. H.; Yersin, H. Organometallic Pt(II) and Ir(III) Triplet Emitters for OLED Applications and the Role of Spin-Orbit Coupling: A Study Based on High-Resolution Optical Spectroscopy. *Top. Organomet. Chem.* **2010**, *29*, 193–235.
- (9) Yersin, H.; Finkenzeller, W. *Highly efficient OLEDs with Phosphorescent Materials*; Yersin, H., Ed.; Wiley-VCH Verlag GmbH & Co. KGaA: Weinheim, 2008; Chapter 1, pp 1–97.
- (10) Deaton, J. C.; Castellano, F. N. *Iridium(III) in Optoelectronic and Photonic Applications*; Zysman-Colman, E., Ed.; Wiley: Chichester, West Sussex, 2017; Chapter 1, pp 1–70.
- (11) Tamayo, A. B.; Garon, S.; Sajoto, T.; Djurovich, P. I.; Tsyba, I. M.; Bau, R.; Thompson, M. E. Cationic Bis-Cyclometalated Iridium(III) Diimine Complexes and Their Use in Efficient Blue, Green, and Red Electroluminescent Devices. *Inorg. Chem.* **2005**, *44*, 8723–8732.
- (12) Costa, R. D.; Monti, F.; Accorsi, G.; Barbieri, A.; Bolink, H. J.; Ortí, E.; Armaroli, N. Photophysical Properties of Charged Cyclometalated Ir(III) Complexes: A Joint Theoretical and Experimental Study. *Inorg. Chem.* **2011**, *50*, 7229–7238.
- (13) Ladouceur, S.; Fortin, D.; Zysman-Colman, E. Enhanced Luminescent Iridium(III) Complexes Bearing Aryltriazole Cyclometalated Ligands. *Inorg. Chem.* **2011**, *50*, 11514–11526.
- (14) Ladouceur, S.; Fortin, D.; Zysman-Colman, E. Role of Substitution on the Photophysical Properties of 5,5'-Diaryl-2,2'-

- bipyridine (bpy*) in [Ir(ppy)₂(bpy*)]PF₆ Complexes: A Combined Experimental and Theoretical Study. *Inorg. Chem.* **2010**, *49*, 5625–5641.
- (15) Sajoto, T.; Djurovich, P. I.; Tamayo, A.; Yousufuddin, M.; Bau, R.; Thompson, M. E.; Holmes, R. J.; Forrest, S. R. Blue and Near-UV Phosphorescence from Iridium Complexes with Cyclometalated Pyrazolyl or N-Heterocyclic Carbene Ligands. *Inorg. Chem.* **2005**, *44*, 7992–8003.
- (16) Haneder, S.; Da Como, E.; Feldmann, J.; Lupton, J. M.; Lennartz, C.; Erk, P.; Fuchs, E.; Molt, O.; Münster, I.; Schildknecht, C.; Wagenblast, G. Controlling the Radiative Rate of Deep-Blue Electrophosphorescent Organometallic Complexes by Singlet-Triplet Gap Engineering. *Adv. Mater.* **2008**, *20*, 3325–3330.
- (17) *Highly Efficient OLEDs with Phosphorescent Materials*; Yersin, H., Ed.; Wiley-VCH Verlag GmbH & Co. KGaA: Weinheim, 2007.
- (18) Longhi, E.; De Cola, L. *Iridium(III) in Optoelectronic and Photonic Applications*; Zysman-Colman, E., Ed.; Wiley: Chichester, West Sussex, 2017; Chapter 6, pp 205–274.
- (19) Prier, C. K.; Rankic, D. A.; MacMillan, D. W. C. Visible Light Photoredox Catalysis with Transition Metal Complexes: Applications in Organic Synthesis. *Chem. Rev.* **2013**, *113*, 5322–5363.
- (20) Arias-Rotondo, D. M.; McCusker, J. K. The Photophysics of Photoredox Catalysis: A Roadmap for Catalyst Design. *Chem. Soc. Rev.* **2016**, *45*, 5803–5820.
- (21) Kagalwala, H. N.; Chirdon, D. N.; Bernhard, S. *Iridium(III) in Optoelectronic and Photonic Applications*; Zysman-Colman, E., Ed.; Wiley: Chichester, West Sussex, 2017; Chapter 12, pp 583–616.
- (22) Monos, T. M.; Stephenson, C. R. J. *Iridium(III) in Optoelectronic and Photonic Applications*; Zysman-Colman, E., Ed.; Wiley: Chichester, West Sussex, 2017; Chapter 11, pp 541–582.
- (23) *Iridium(III) in Optoelectronic and Photonic Applications*; Zysman-Colman, E., Ed.; Wiley: Chichester, West Sussex, 2017.
- (24) Sandrini, D.; Maestri, M.; Ziessel, R. Spectroscopic Behavior of a New Family of Mixed-Ligand Iridium(III) Complexes. *Inorg. Chim. Acta* **1989**, *163*, 177–180.
- (25) Suenobu, T.; Guldi, D. M.; Ogo, S.; Fukuzumi, S. Excited-State Deprotonation and H/D Exchange of an Iridium Hydride Complex. *Angew. Chem., Int. Ed.* **2003**, *42*, 5492–5495.
- (26) Ziessel, R. Efficient homogeneous photochemical water gas shift reaction catalysed under extremely mild conditions by novel iridium(III) complexes: $[(\eta^5\text{-Me}_5\text{C}_5)\text{Ir}(\text{bpy})\text{Cl}]^+$, $[(\eta^5\text{-Me}_5\text{C}_5)\text{Ir}(\text{bpy})\text{H}]^+$, and $[(\eta^5\text{-Me}_5\text{C}_5)\text{Ir}(\text{phen})\text{Cl}]^+$ (bpy = 2,2'-bipyridine; phen = 1,10-phenanthroline). *J. Chem. Soc., Chem. Commun.* **1988**, 16–17.
- (27) Ziessel, R. Photocatalysis of the Homogeneous Water-Gas Shift Reaction under Ambient Conditions by Cationic Iridium(III) Complexes. *Angew. Chem., Int. Ed.* **1991**, *30*, 844–847.
- (28) Ziessel, R. Photocatalysis. Mechanistic studies of homogeneous photochemical water gas shift reaction catalyzed under mild conditions by novel cationic iridium(III) complexes. *J. Am. Chem. Soc.* **1993**, *115*, 118–127.
- (29) Brereton, K. R.; Bonn, A. G.; Miller, A. J. M. Molecular Photoelectrocatalysts for Light-Driven Hydrogen Production. *ACS Energy Lett.* **2018**, *3*, 1128–1136.
- (30) Pitman, C. L.; Miller, A. J. M. Molecular Photoelectrocatalysts for Visible Light-Driven Hydrogen Evolution from Neutral Water. *ACS Catal.* **2014**, *4*, 2727–2733.
- (31) Chambers, M. B.; Kurtz, D. A.; Pitman, C. L.; Brennaman, M. K.; Miller, A. J. M. Efficient Photochemical Dihydrogen Generation Initiated by a Bimetallic Self-Quenching Mechanism. *J. Am. Chem. Soc.* **2016**, *138*, 13509–13512.
- (32) Barrett, S. M.; Slattery, S. A.; Miller, A. J. M. Photochemical Formic Acid Dehydrogenation by Iridium Complexes: Understanding Mechanism and Overcoming Deactivation. *ACS Catal.* **2015**, *5*, 6320–6327.
- (33) Barrett, S. M.; Pitman, C. L.; Walden, A. G.; Miller, A. J. M. Photoswitchable Hydride Transfer from Iridium to 1-Methylnicotinamide Rationalized by Thermochemical Cycles. *J. Am. Chem. Soc.* **2014**, *136*, 14718–14721.
- (34) Pitman, C. L.; Miller, A. J. M. Photochemical Production of Ethane from an Iridium Methyl Complex. *Organometallics* **2017**, *36*, 1906–1914.
- (35) Tsuboyama, A.; Iwawaki, H.; Furugori, M.; Mukaide, T.; Kamatani, J.; Igawa, S.; Moriyama, T.; Miura, S.; Takiguchi, T.; Okada, S.; Hoshino, M.; Ueno, K. Homoleptic Cyclometalated Iridium Complexes with Highly Efficient Red Phosphorescence and Application to Organic Light-Emitting Diode. *J. Am. Chem. Soc.* **2003**, *125*, 12971–12979.
- (36) Deaton, J. C.; Young, R. H.; Lenhard, J. R.; Rajeswaran, M.; Huo, S. Photophysical Properties of the Series *fac*- and *mer*-(1-Phenylisoquinolino-N⁺C^{2'})_x(2-phenylpyridinato-N⁺C^{2'})_{3-x}Iridium(III) ($x = 1-3$). *Inorg. Chem.* **2010**, *49*, 9151–9161.
- (37) Li, L.; Brennessel, W. W.; Jones, W. D. An Efficient Low-Temperature Route to Polycyclic Isoquinoline Salt Synthesis via C–H Activation with [Cp*₂MCl₂]₂ (M = Rh, Ir). *J. Am. Chem. Soc.* **2008**, *130*, 12414–12419.
- (38) Park-Gehrke, L. S.; Freudenthal, J.; Kaminsky, W.; DiPasquale, A. G.; Mayer, J. M. Synthesis and oxidation of Cp*₂Ir^{III} compounds: functionalization of a Cp* methyl group. *Dalton Trans.* **2009**, 1972–1983.
- (39) Brewster, T. P.; Miller, A. J. M.; Heinekey, D. M.; Goldberg, K. I. Hydrogenation of Carboxylic Acids Catalyzed by Half-Sandwich Complexes of Iridium and Rhodium. *J. Am. Chem. Soc.* **2013**, *135*, 16022–16025.
- (40) Xiao, X.-Q.; Jin, G.-X. Functionalized N-Heterocyclic Carbene Iridium Complexes: Synthesis, Structure and Addition Polymerization of Norbornene. *J. Organomet. Chem.* **2008**, *693*, 3363–3368.
- (41) Shavaleev, N. M.; Monti, F.; Scopelliti, R.; Baschieri, A.; Sambri, L.; Armaroli, N.; Grätzel, M.; Nazeeruddin, M. K. Extreme Tuning of Redox and Optical Properties of Cationic Cyclometalated Iridium(III) Isocyanide Complexes. *Organometallics* **2013**, *32*, 460–467.
- (42) Yang, C.-H.; Cheng, Y.-M.; Chi, Y.; Hsu, C.-J.; Fang, F.-C.; Wong, K.-T.; Chou, P.-T.; Chang, C.-H.; Tsai, M.-H.; Wu, C.-C. Blue-Emitting Heteroleptic Iridium(III) Complexes Suitable for High-Efficiency Phosphorescent OLEDs. *Angew. Chem., Int. Ed.* **2007**, *46*, 2418–2421.
- (43) Coppo, P.; Plummer, E. A.; De Cola, L. Tuning iridium(III) phenylpyridine complexes in the “almost blue” region. *Chem. Commun.* **2004**, 1774–1775.
- (44) Yang, C.-H.; Mauro, M.; Polo, F.; Watanabe, S.; Muenster, I.; Fröhlich, R.; De Cola, L. Deep-Blue-Emitting Heteroleptic Iridium(III) Complexes Suited for Highly Efficient Phosphorescent OLEDs. *Chem. Mater.* **2012**, *24*, 3684–3695.
- (45) Vanhelmont, F. W. M.; Güdel, H. U. Synthesis, Crystal Structure, High-Resolution Optical Spectroscopy, and Extended Hückel Calculations for [Re(CO)₄(thpy)] (thpy = 2-(2-Thienyl)pyridinate). Comparison with Related Cyclometalated Complexes. *Inorg. Chem.* **1997**, *36*, 5512–5517.
- (46) Colombo, M.; Hauser, A.; Güdel, H. U. Competition Between Ligand Centered and Charge Transfer Lowest Excited States in Bis Cyclometalated Rh³⁺ and Ir³⁺ Complexes. *Top. Curr. Chem.* **1994**, *171*, 144–171.
- (47) Maity, A.; Le, L. Q.; Zhu, Z.; Bao, J.; Teets, T. S. Steric and Electronic Influence of Aryl Isocyanides on the Properties of Iridium(III) Cyclometalates. *Inorg. Chem.* **2016**, *55*, 2299–2308.
- (48) Teets, H.; Rausch, A. F.; Czerwieńec, R. *Physics of Organic Semiconductors*, 2nd ed.; Brütting, W., Adachi, C., Eds.; Wiley-VCH Verlag GmbH & Co. KGaA: Weinheim, 2012; Chapter 13, pp 371–424.
- (49) Flynn, C. M., Jr.; Demas, J. N. Synthesis and luminescence of the tris(2,2'-bipyridine)iridium(III) ion. *J. Am. Chem. Soc.* **1974**, *96*, 1959–1960.
- (50) Colombo, M. G.; Hauser, A.; Guedel, H. U. Evidence for strong mixing between the LC and MLCT excited states in bis(2-phenylpyridinato-C²,N')(2,2'-bipyridine)iridium(III). *Inorg. Chem.* **1993**, *32*, 3088–3092.

- (51) Krausz, E.; Higgins, J.; Riesen, H. The apparent "dual emitter" characteristics of iridium bipyridine phenanthroline complexes, $[\text{Ir}(\text{bpy})_x(\text{phen})_{3-x}]^{3+}$ for $x = 1, 2$. *Inorg. Chem.* **1993**, *32*, 4053–4056.
- (52) Rausch, A. F.; Thompson, M. E.; Yersin, H. Matrix Effects on the Triplet State of the OLED Emitter $\text{Ir}(4,6\text{-dFppy})_2(\text{pic})$ (FIrpic): Investigations by High-Resolution Optical Spectroscopy. *Inorg. Chem.* **2009**, *48*, 1928–1937.
- (53) Rausch, A. F.; Thompson, M. E.; Yersin, H. Blue Light Emitting Ir(III) Compounds for OLEDs - New Insights into Ancillary Ligand Effects on the Emitting Triplet State. *J. Phys. Chem. A* **2009**, *113*, 5927–5932.
- (54) Bauer, R.; Finkenzeller, W. J.; Bogner, U.; Thompson, M. E.; Yersin, H. Matrix influence on the OLED emitter $\text{Ir}(\text{btp})_2(\text{acac})$ in polymeric host materials - Studies by persistent spectral hole burning. *Org. Electrochem.* **2008**, *9*, 641–648.
- (55) Kohlrausch, R. Theorie des elektrischen Rückstandes in der Leidener Flasche. *Ann. Phys. Chem.* **1854**, *167*, 179–214.
- (56) Berberan-Santos, M. N.; Bodunov, E. N.; Valeur, B. Mathematical functions for the analysis of luminescence decays with underlying distributions 1. Kohlrausch decay function (stretched exponential). *Chem. Phys.* **2005**, *315*, 171–182.
- (57) Thompson, D. W.; Fleming, C. N.; Myron, B. D.; Meyer, T. J. Rigid Medium Stabilization of Metal-to-Ligand Charge Transfer Excited States. *J. Phys. Chem. B* **2007**, *111*, 6930–6941.
- (58) McGoorty, M. M.; Khnazyer, R. S.; Castellano, F. N. Enhanced photophysics from self-assembled cyclometalated Ir(III) complexes in water. *Chem. Commun.* **2016**, *52*, 7846–7849.
- (59) Castellano, F. N.; Heimer, T. A.; Tandhasetti, M. T.; Meyer, G. J. Photophysical Properties of Ruthenium Polypyridyl Photonic SiO₂ Gels. *Chem. Mater.* **1994**, *6*, 1041–1048.
- (60) MedCalc Statistical Software Version 17.5; MedCalc Software BVBA: Ostend, Belgium, 2016; <https://www.medcalc.org>.
- (61) Harrigan, R. W.; Crosby, G. A. Symmetry assignments of the lowest CT excited states of ruthenium (II) complexes via a proposed electronic coupling model. *J. Chem. Phys.* **1973**, *59*, 3468–3476.
- (62) Hager, G. D.; Crosby, G. A. Charge-transfer excited states of ruthenium(II) complexes. I. Quantum yield and decay measurements. *J. Am. Chem. Soc.* **1975**, *97*, 7031–7037.
- (63) Yersin, H.; Rausch, A. F.; Czerwiniak, R.; Hofbeck, T.; Fischer, T. The triplet state of organo-transition metal compounds. Triplet harvesting and singlet harvesting for efficient OLEDs. *Coord. Chem. Rev.* **2011**, *255*, 2622–2652.
- (64) Lumpkin, R. S.; Kober, E. M.; Worl, L. A.; Murtaza, Z.; Meyer, T. J. Metal-to-Ligand Charge-Transfer (MLCT) Photochemistry: Experimental Evidence for the Participation of a Higher Lying MLCT State in Polypyridyl Complexes of Ruthenium(II) and Osmium(II). *J. Phys. Chem.* **1990**, *94*, 239–243.
- (65) Endo, A.; Suzuki, K.; Yoshihara, T.; Tobita, S.; Yahiro, M.; Adachi, C. Measurement of Photoluminescence Efficiency of Ir(III) Phenylpyridine Derivatives in Solution and Solid-State Films. *Chem. Phys. Lett.* **2008**, *460*, 155–157.
- (66) Garakyaraghi, S.; Crapps, P. D.; McCusker, C. E.; Castellano, F. N. Cuprous Phenanthroline MLCT Chromophore Featuring Synthetically Tailored Photophysics. *Inorg. Chem.* **2016**, *55*, 10628–10636.
- (67) Maruszewski, K.; Kincaid, J. R. Dramatic Increase of 3MLCT State Lifetimes of a Ruthenium(II) Polypyridine Complex upon Entrapment within Y-Zeolite Supercages. *Inorg. Chem.* **1995**, *34*, 2002–2006.
- (68) Sykora, M.; Kincaid, J. R. Synthetic Manipulation of Excited State Decay Pathways in a Series of Ruthenium(II) Complexes Containing Bipyrazine and Substituted Bipyridine Ligands. *Inorg. Chem.* **1995**, *34*, 5852–5856.
- (69) Bhuiyan, A. A.; Kincaid, J. R. Synthesis and Photophysical Properties of Zeolite-Entrapped Bisterpyridine Ruthenium(II). Dramatic Consequences of Ligand-Field-State Destabilization. *Inorg. Chem.* **1998**, *37*, 2525–2530.
- (70) Kober, E. M.; Meyer, T. J. An electronic structural model for the emitting MLCT excited states of $\text{Ru}(\text{bpy})_3^{2+}$ and $\text{Os}(\text{bpy})_3^{2+}$. *Inorg. Chem.* **1984**, *23*, 3877–3886.
- (71) Nozaki, K. Theoretical Studies on $\text{Ir}(\text{ppy})_3$. *J. Chin. Chem. Soc.* **2004**, *53*, 101–112.
- (72) Finkenzeller, W. J.; Yersin, H. Emission of $\text{Ir}(\text{ppy})_3$. Temperature dependence, decay dynamics, and magnetic field properties. *Chem. Phys. Lett.* **2003**, *377*, 299–305.
- (73) Colombo, M. G.; Hauser, A.; Güdel, H. U. Competition Between Ligand Centered and Charge Transfer Lowest Excited States in Bis Cyclometalated Rh^{3+} and Ir^{3+} Complexes. *Top. Curr. Chem.* **1994**, *171*, 144–171.
- (74) Finkenzeller, W. J.; Stöbel, P.; Yersin, H. Emission and absorption of $\text{Ir}(\text{ppy})_2(\text{CO})(\text{Cl})$ - temperature dependence, phosphorescence decay dynamics, and assignment of excited states. *Chem. Phys. Lett.* **2004**, *397*, 289–295.
- (75) Brereton, K. R.; Bonn, A. G.; Miller, A. J. M. Molecular Photoelectrocatalysts for Light-Driven Hydrogen Production. *ACS Energy Lett.* **2018**, *3*, 1128–1136.
- (76) White, C.; Yates, A.; Maitlis, P. M.; Heinekey, D. M. η^5 -(Pentamethylcyclopentadienyl)Rhodium and -Iridium Compounds. *Inorg. Synth.* **1992**, *29*, 228–230.
- (77) Sattler, W.; Henling, L. M.; Winkler, J. R.; Gray, H. B. Bespoke Photoreductants: Tungsten Arylisocyanides. *Inorg. Chem.* **2015**, *137*, 1198–1205.
- (78) Frisch, M. J.; Trucks, G. W.; Schlegel, H. B.; Scuseria, G. E.; Robb, M. A.; Cheeseman, J. R.; Scalmani, G.; Barone, V.; Mennucci, B.; Petersson, G. A.; Nakatsuji, H.; Caricato, M.; Li, X.; Hratchian, H. P.; Izmaylov, A. F.; Bloino, J.; Zheng, G.; Sonnenberg, J. L.; Hada, M.; Ehara, M.; Toyota, K.; Fukuda, R.; Hasegawa, J.; Ishida, M.; Nakajima, T.; Honda, Y.; Kitao, O.; Nakai, H.; Vreven, T.; Montgomery, J. A., Jr.; Peralta, J. E.; Ogliaro, F.; Bearpark, M.; Heyd, J. J.; Brothers, E.; Kudin, K. N.; Staroverov, V. N.; Kobayashi, R.; Normand, J.; Raghavachari, K.; Rendell, A.; Burant, J. C.; Iyengar, S. S.; Tomasi, J.; Cossi, M.; Rega, N.; Millam, J. M.; Klene, M.; Knox, J. E.; Cross, J. B.; Bakken, V.; Adamo, C.; Jaramillo, J.; Gomperts, R.; Stratmann, R. E.; Yazyev, O.; Austin, A. J.; Cammi, R.; Pomelli, C.; Ochterski, J. W.; Martin, R. L.; Morokuma, K.; Zakrzewski, V. G.; Voth, G. A.; Salvador, P.; Dannenberg, J. J.; Dapprich, S.; Daniels, A. D.; Farkas, Ö.; Foresman, J. B.; Ortiz, J. V.; Cioslowski, J.; Fox, D. J. *Gaussian 09*, Revision D.01; Gaussian, Inc.: Wallingford CT, 2009.
- (79) Becke, A. D. Density-functional thermochemistry. III. The role of exact exchange. *J. Chem. Phys.* **1993**, *98*, 5648–5652.
- (80) Lee, C.; Yang, W.; Parr, R. G. Development of the Colle-Salvetti Correlation-Energy Formula into a Functional of the Electron Density. *Phys. Rev. B: Condens. Matter Mater. Phys.* **1988**, *37*, 785–789.
- (81) Grimme, S.; Antony, J.; Ehrlich, S.; Krieg, H. A Consistent and Accurate Ab Initio Parametrization of Density Functional Dispersion Correction (DFT-D) for the 94 elements H-Pu. *J. Chem. Phys.* **2010**, *132*, 154104.
- (82) Hay, P. J.; Wadt, W. R. Ab initio effective core potentials for molecular calculations. Potentials for K to Au including the outermost core orbitals. *J. Chem. Phys.* **1985**, *82*, 299–310.
- (83) Ehlers, A. W.; Böhme, M.; Dapprich, S.; Gobbi, A.; Höllwarth, A.; Jonas, V.; Köhler, K. F.; Stegmann, R.; Veldkamp, A.; Frenking, G. A set of f-polarization functions for pseudo-potential basis sets of the transition metals ScCu, YAg and LaAu. *Chem. Phys. Lett.* **1993**, *208*, 111–114.
- (84) Hehre, W. J.; Stewart, R. F.; Pople, J. A. Self-Consistent Molecular-Orbital Methods. I. Use of Gaussian Expansions of Slater-Type Atomic Orbitals. *J. Chem. Phys.* **1969**, *51*, 2657–2664.
- (85) Krishnan, R.; Binkley, J. S.; Seeger, R.; Pople, J. A. Self-consistent molecular orbital methods. XX. A basis set for correlated wave functions. *J. Chem. Phys.* **1980**, *72*, 650–654.
- (86) Marenich, A. V.; Cramer, C. J.; Truhlar, D. G. Universal Solvation Model Based on Solute Electron Density and on a Continuum Model of the Solvent Defined by the Bulk Dielectric

Constant and Atomic Surface Tensions. *J. Phys. Chem. B* **2009**, *113*, 6378–6396.

(87) Lu, T.; Chen, F. Multiwfn: A multifunctional wavefunction analyzer. *J. Comput. Chem.* **2012**, *33*, 580–592.